sustainability

MDPI

Article

Quantifying the Impacts of Climate and Land Cover Changes on the Hydrological Regime of a Complex Dam Catchment Area

Muhammad Umer Masood [1], Saif Haider [2,3], Muhammad Rashid [2], Mohammed Suleman Aldlemy [4,5,*], Chaitanya B. Pande [3,6,7,*], Bojan Đurin [8], Raad Z. Homod [9], Fahad Alshehri [3] and Ismail Elkhrachy [10]

1 Geological Engineering Department, Montana Technological University, Butte, MT 59701, USA
2 Centre of Excellence in Water Resources Engineering, University of Engineering and Technology, Lahore 54890, Pakistan
3 Abdullah Alrushaid Chair for Earth Science Remote Sensing Research, Geology and Geophysics Department, College of Science, King Saud University, Riyadh 11451, Saudi Arabia; falshehria@ksu.edu.sa
4 Department of Mechanical Engineering, Collage of Mechanical Engineering Technology, Benghazi 16063, Libya
5 Center for Solar Energy Research and Studies (CSERS), Benghazi 16063, Libya
6 Institute of Energy Infrastructure, University Tenaga Nasional, Kajang 43000, Malaysia
7 New Era and Development in Civil Engineering Research Group, Scientific Research Center, Al-Ayen University, Thi-Qar, Nasiriyah 64001, Iraq
8 Department of Civil Engineering, University North, 48000 Koprivnica, Croatia; bdjurin@unin.hr
9 Department of Oil and Gas Engineering, Basrah University for Oil and Gas, Basra 61004, Iraq
10 Civil Engineering Department, College of Engineering, Najran University, King Abdulaziz Road, Najran 66454, Saudi Arabia; iaelkhrachy@nu.edu.sa
* Correspondence: maldlemy@ceb.edu.ly (M.S.A.); chaitanay45@gmail.com (C.B.P.)

Abstract: In this study, hydrological modeling at the watershed level is used to assess the impacts of climate and land use changes on the catchment area of the Khanpur Dam, which is an important water source for Rawalpindi and Islamabad. The hydrological impact of past and anticipated precipitation in the Khanpur Dam watershed was forecast by using a HEC-HMS model. After calibration, the framework was employed to analyze the effects of changes in land cover and climate on the hydrological regime. The model used information from three climatic gauge stations (Murree, Islamabad Zero Point, and Khanpur Dam) to split the Khanpur Dam catchment area into five sub-basins that encompass the entire watershed region, each with distinctive characteristics. The model was evaluated and checked for 2016–2018 and 2019–2020, and it produced an excellent match with the actual and anticipated flows. After statistical downscaling with the CMhyd model, the most effective performing GCM (MPI-ESM1-2-HR) among the four GCMs was chosen and used to forecast projections of temperature and precipitation within two shared socioeconomic pathways (SSP2 and SSP5). The predictions and anticipated changes in land cover were incorporated into the calibrated HEC-HMS model to evaluate the potential impact of climate change and land cover change at the Khanpur Dam. The starting point era (1990–2015) and the projected period (2016–2100), which encompassed the basis in the present century, were analyzed annually. The results indicated a spike in precipitation for the two SSPs, which was predicted to boost inflows all year. Until the end of the twenty-first century, SSP2 predicted a 21 percent rise in precipitation in the Khanpur Dam catchment area, while SSP5 predicted a 28% rise in precipitation. Increased flows were found to be projected in the future. It was found that the calibrated model could also be used effectively for upcoming studies on hydrological effects on inflows of the Khanpur Dam basin.

Keywords: land cover alteration; Khanpur Dam; climate change; GCMs; statistical downscaling; CA Markov; HEC-HMS

check for updates

Citation: Masood, M.U.; Haider, S.; Rashid, M.; Aldlemy, M.S.; Pande, C.B.; Đurin, B.; Homod, R.Z.; Alshehri, F.; Elkhrachy, I. Quantifying the Impacts of Climate and Land Cover Changes on the Hydrological Regime of a Complex Dam Catchment Area. *Sustainability* **2023**, *15*, 15223. https://doi.org/10.3390/su152115223

Academic Editor: Francesco Faccini

Received: 16 September 2023
Revised: 19 October 2023
Accepted: 20 October 2023
Published: 24 October 2023

1. Introduction

It is essential to ensure that everyone survives as well as social and economic growth under the scarcity of water reserves. Rising population and development initiatives have put stress on the world's water supplies [1]. Globally, water extraction has grown six times during the last century, which has been twice the rate of population growth. Five hundred million people may soon be affected by a physical water crisis that affects a quarter of all the people on Earth [2]. Estimates indicate that more than 65 percent of the waterways and pond habitats are under severe threat [3]. Globally, Pakistan ranks 36th among the countries with the least water shortage. The current steady water source in Pakistan is 191 MAF, yet by 2025, demand is expected to increase to 274 MAF [4]. Surface water runoff delivers the bulk of water required for use in homes and farms.

Still, there are significant changes in global surface water runoff [5]. Surface water runoff fluctuations are believed to be mostly impacted by human activities and changing environments [4–8]. The deteriorating state of Pakistan's water table indicates the dire future of the country's agricultural and residential sectors as well as its manufacturing sector. As a worldwide threat, drought may lead to a number of negative outcomes, such as worsening soil state, forest fires, lower crop productions, as well as poor water and air quality. Due to global warming, the length, size, and dispersion of droughts have each risen over the past few decades, which has worsened their negative impacts. Anthropogenic activities, often known as human-caused environmental disturbances, include consumption of freshwater for agriculture and manufacturing, as well as the development, deforestation, and modifications regarding land cover [9–13]. Understanding how and if changes in the environment and human activities combine to modify streamflow is challenging, particularly in local regions. Therefore, for more efficient water utilization, it is crucial to comprehend local and regional effects of these changes. Researchers have developed a number of methodologies for understanding responses of runoff to changes in environment and land usage. The approaches include hydrological simulations, statistical methods, and matched basin methods. All of the methods include pros and cons. For example, in hydrological modeling, dispersed, semi-distributed, and lumped models are frequently utilized; however, due to the necessity for numerous entries during the calibration and validation procedures, such models cannot be utilized for circumstances when there is limited information. It is difficult to evaluate the consequences of changes in land cover explicitly, while statistics only offer a variety of geographical explanations. In contrast, by employing matched basin approaches, it is difficult to separate two basins that exhibit similar features [14]. Additionally, there are only a few options for quarterly water equilibrium that are simple to calibrate and validate. These models also have a logical foundation and need less information [15]. The ABCD hydrological approach has been recognized to be an effective model for identifying monthly temporal streamflow values. The ABCD hydrological method outperforms other hydrological models due to its simpler structure [16]. An ABCD model requires less effort to obtain values [17]. It is often employed in studies to look at the local equilibrium of water because of its simple structure. This arrangement is easier to operate and it offers an easy-to-understand design [18]. Reservoir workers, nevertheless, use reservoir operating regulations as a general framework for guidelines when determining the volume and timing of water discharge. Simply, to correctly determine the retention capacity for a certain time of year, the person in charge has to discharge water when required. These guidelines, which may assume the shape of a curve or group of spirals, are often based upon careful examination of more important hydrological criteria and circumstances in descending order. The effectiveness of operating regulations can be significantly impacted by a large modification in the amount or manner of ingestion. The implications of changes in climate can be, at least, substantially mitigated by adaptation, i.e., by continuously adopting steps to lessen the vulnerability to climate change. These are some of the limitations to its effectiveness in environmental degradation, which is occurring more quickly and over bigger scales.

Reducing the likelihood of catastrophes requires developing workable adaptation techniques and addressing the severity of climate change. Every industry has adaptation options, but their abilities to lower risks related to environmental change differ among industries and regions. Scholars have conducted many investigations on the management of water resources to more fully comprehend and to effectively regulate the potential impacts of environmental change and land use change on the hydrological regimes of various watersheds [8,19–26]. However, these analyses have not revealed how changes in inflows may impact the operational approaches used to manage various reservoirs. Variations in streamflow can have a direct influence on water availability, affecting a variety of industries and sectors, including agriculture, industry, and household water supply.

For simulations of rainfall and discharge, semi-distributed hydrodynamic theoretical framework HEC-HMS models are widely employed [27–29]. A HEC-HMS model employs conventional methods to model runoff in both immediate and future circumstances [30,31]. According to other research, HEC-HMS models can simulate streamflow utilizing readily accessible facts and various catchment types [32–35]. To investigate whether changes in the environment and land use can affect the runoff trend, a number of researchers have also used HEC-HMS models for predicting runoff and precipitation. The results obtained utilizing HEC-HMS models worldwide have been appropriate for attribution purposes [36,37]. Therefore, an attribution analysis was performed in the current study utilizing a HEC-HMS model. Researchers and administrators of water resources utilize various techniques and frameworks for the provenance of assessments. Nevertheless, there is bound to be certain unknowns and disparities because each approach and perspective yields results that vary [38,39].

In the current study, the consequences of anthropogenic activities and warming temperatures are considered separately, since watersheds are especially susceptible to the impacts of environmental transitions and human activities in moist surroundings [40]. Therefore, the Khanpur Dam catchment area, an oppressive Margalla Foothills basin, is the focus of the current study. This basin's water supply is primarily utilized to provide drinking water to adjacent municipalities, including Islamabad's metropolis. The land usage in this basin has seen significant change during the previous years. The primary goals of this investigation are as follows: (a) To compare various statistical downscaling strategies and to downscale future temperature and precipitation estimates using GCM data; (b) to estimate, using a hydrological model, the effects of future climate change and land cover change on streamflow at the Potohar Plateau basin under CMIP6 models.

2. Study Area

The Khanpur Dam was constructed at 33°48′06″ N and 72°55′50″ E, on the Haro River; Khyber Pakhtunkhwa (KPK) and the capital region are its catchment areas. Its perimeter is 232.4 km, and its catchment area is 783.82 km^2. The height of the Khanpur Dam is 50.9 m, its volume of storage is 130.7 Mm^3, and its design flood is 5153 m^3 per second. It has a 501.81 km^2 gross command area, of which 147.58 km^2 are culturable command areas. It delivers irrigation water at a rate of 11.52 m^3 per second to the districts of Attock and Rawalpindi. It supplies water at a rate of 5.37 m^3 per second to Rawalpindi and Islamabad. The Murree, Ayubia, and Margalla Hills are the mountains from whence the Haro River rises. Four significant tributaries feed the river, including Lora Haro, Stora Haro, Neelan, and Kunhad. The river is filled as a result of precipitation, with some elements coming from snowmelt. The Islamabad and Murree rain gauge stations are the nearest meteorological stations to the catchment area. The Khanpur Dam catchment area is shown in Figure 1. The Khanpur Dam is a popular location for day trips outside of the twin cities of Islamabad and Rawalpindi. People visit the area for picnics and to participate in a variety of sports including swimming, paragliding, boating, etc.

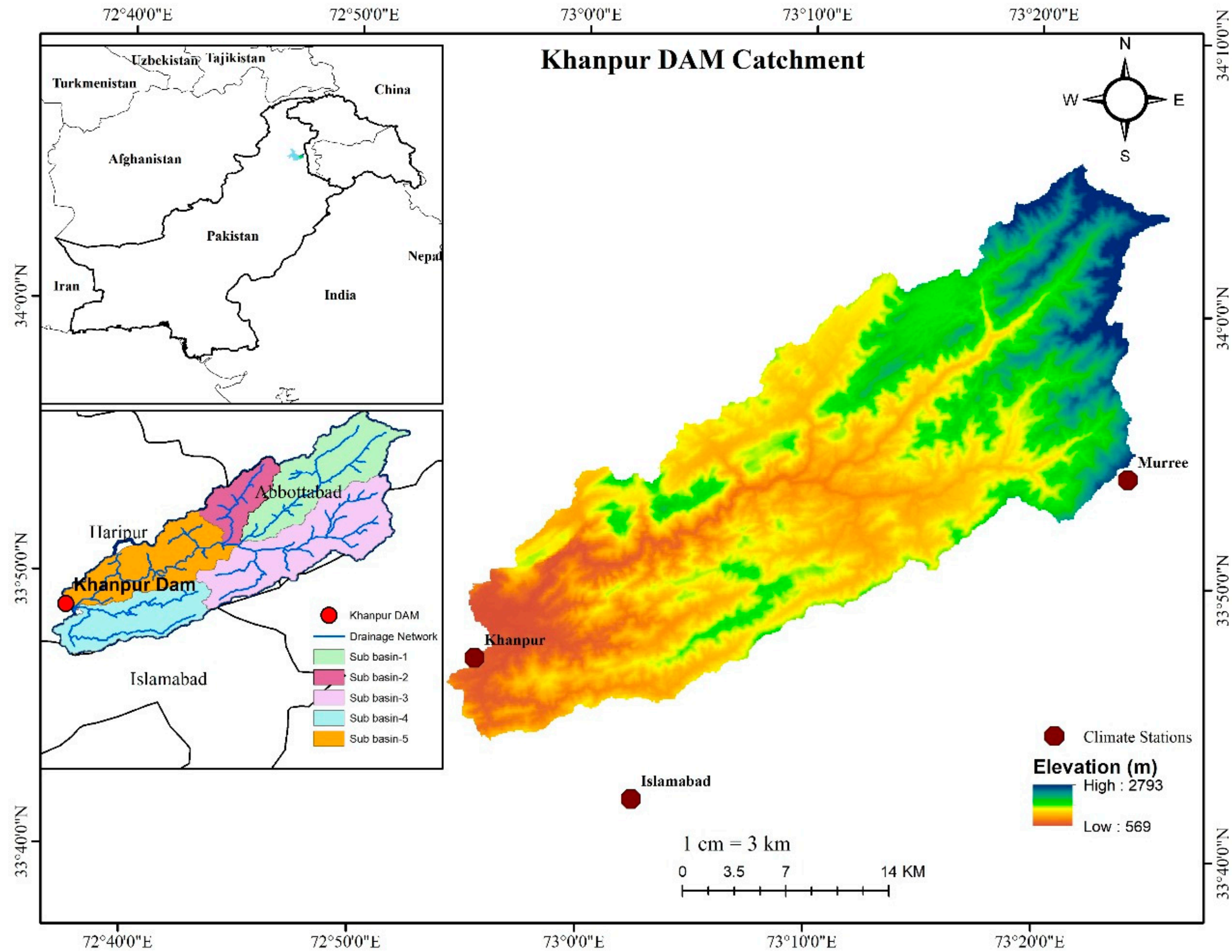

Figure 1. Statistics of the Khanpur Dam catchment area's region and altitude.

3. Materials and Methods

3.1. Datasets

3.1.1. Hydro-Meteorological Data

Three climate locations provided the information on rainfall. The Pakistan Meteorological Department (PMD) provided daily data for the sites of Islamabad (zero point), Murree, and the Khanpur Dam between 1990 and 2015. As a baseline, all three sites utilized historical data from 1990 to 2015.

3.1.2. Satellite Data

A DEM of the Khanpur Dam and its catchment area, at resolution 30 m, was provided by the USGS Earth Explorer together with Landsat images for identifying the Khanpur Dam basin and deriving physiological traits such as height, gradient, and catchment area.

The present research used imagery from Landsat 8 (OLI) and Landsat 4–5 (TM), employing bands 8 and 7, respectively, to differentiate among changes of land cover inside the Khanpur Dam catchment area for three separate eras, i.e., 2000, 2013, and 2023. Temporal geographic spread and greenery variety were given attention while determining the image's durations. All images were downloaded from the USGS Earth Explorer website as TIFF files.

3.1.3. Climate Anticipated Data

Among the four GCMs, the MPI-ESM1-2-HR global circulation model, with the most effective performance, was selected for this research to predict climate during two shared socioeconomic pathways (SSPs), i.e., SSP2 and SSP5. Information about this GCM can be found in the sixth assessment report of the IPCC. To forecast localized weather circumstances, massive GCM data were reduced to resemble a grid. Statistical downscaling was performed by establishing quantitative correlations between the small-scale GCM climate variables and the regional climate variables. Downscaling statistics is significantly easier than comprehensive dynamic downscaling. However, for statistical downscaling, past climate data and measured data are crucial. For this work, a distribution mapping (multiplicative for precipitation and addition for temperature) approach was employed in order to scale down temperature and precipitation.

Based on the effectiveness of several bias correction strategies, the bias correction strategies selected and applied for the current work were distribution mapping (DM) for temperature and power transformation for precipitation. The task of transforming analyzed values to GCM monthly average numbers requires replications as its main operating concept. To balance discrepancy caused by downscaling, the GCM statistics, gamma shift functions, and Gaussian transference functions of both temperature and precipitation information, accordingly, must be scaled down.

3.2. Methodology

The present investigation used a methodical approach to identify how Pakistan's Khanpur Dam's hydrological regime has been affected by changes in climatic conditions and land cover. The approach involved gathering information, downloading the GCM imitated weather information, downscaling the results for the Khanpur Dam catchment area, performing hydrological simulations, and amalgamating different variables with the goal to obtain an in-depth comprehension of the intricate relationships and consequences for managing water resources. Figure 2 shows the methodology flowchart used in this investigation.

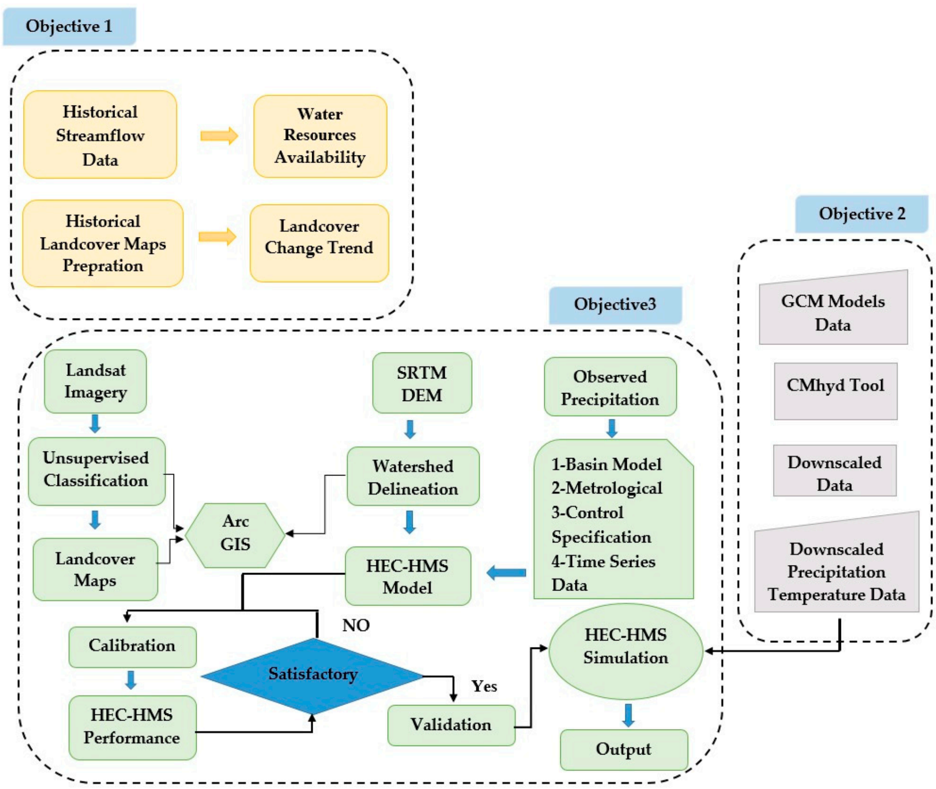

Figure 2. Schematic workflow of the current study.

3.2.1. Statistical Downscaling

Global climate models (GCMs), also known as general circulation models, are powerful tools that are used in climate science to simulate and to predict the Earth's climate system. GCMs incorporate complex mathematical representations of the physical and chemical processes governing the atmosphere, oceans, land surfaces, and sea ice. These models provide a global-scale perspective on climate patterns, helping us to understand large-scale climate dynamics, such as the impacts of greenhouse gas emissions on global temperature trends. However, GCMs operate at relatively coarse spatial resolutions, which can limit their ability to capture regional and local climate variations. To bridge this gap and to provide more localized climate information, researchers often turn to statistical downscaling techniques, which help translate GCM outputs into finer-scale projections tailored to specific regions or locations. Statistical downscaling methods play a crucial role in assessing the potential impacts of climate change at a local scale, and therefore they are an essential component of climate research and adaptation planning.

At the scale of a river basin, the CMhyd framework has been employed to bias correct GCM-based estimates of weather and rainfall [41,42]; in many parts of the world, it has been utilized to lessen the bias among gauge-based real climate factors, as it relies on GCM-forecasted climate data [43]. Employing the CMhyd approach, hydro-climatological investigations, regardless of the river system area, can effectively and consistently reduce the results generated by the GCM, according to the results of a study by Anandhi et al. [43]. CMhyd offers a wide range of statistical methods for downsizing temperature and precipitation. For this work, the GCM results for temperature in the SSP2 and SSP5 scenarios were downscaled using the power transformation method, and regarding rainfall, the distribution mapping approach was followed. In this context, daily time series of pr, tmax, and tmin throughout the baseline period (1990–2015) and research prospective timeline (2016–2100) were combined to provide a temporal trend of everyday information for predicting precipitation (pr), lowest temperature (tmin), and highest temperature (tmax). This information also included projected GCM calculations.

A statistical downscaling approach, called distribution mapping, can be used to make connections among data on worldwide climate and observed local factors for calculating local-scale climate variables. It includes projecting downscaled climate projections to smaller spatial scales by projecting the measured local factor distribution to a massive climatic parameter distribution of probabilities system. To determine nonlinear correlations between large-scale and regional-scale climatic factors, power transformation is a statistical downscaling approach which includes altering information employing power functions. Power transformation makes it possible to better understand the relationships among variables and to capture nonlinearities, allowing for a more precise reduction in weather estimation scale.

3.2.2. Categorization of Images

A poorly supervised image classification technique was used to build images of both present and past LULC. The iso-cluster unsupervised image categorization technique was used to download seven classes, i.e., water bodies, vegetation, dense vegetation, flooded vegetation, shrub and scrub, built-up areas, and bare land, which is a well-known unsupervised image categorization approach for dividing and classifying picture data according to spectral characteristics. ArcGIS was employed to evaluate multiple decades of satellite footage, which works by repeatedly creating clusters from pixels with similar spectral properties. To distinguish separate areas or objects inside an image, IsoCluster uses statistical features of picture information, like spectral data or the intensities of pixels' fingerprints. The program selects the initial cluster centers at random, and then places the pixels in the closest cluster according to their spectral similarity. Finally, cluster centers are changed according to the mean of pixels sent to every group. In order to ensure that pixels are correctly grouped into clusters, this process is repeated until convergence is reached. IsoCluster is especially effective when there is a distinct contrast in spectral properties of various areas or items in a picture, making it a helpful tool for tasks like land cover categorization, recognition of objects, and separation of pictures.

3.2.3. Hydrological Modeling

In this study, the Khanpur Dam catchment area was divided into five sub-basins based on several crucial considerations. Firstly, the subdivision helped to strike a balance between achieving hydrological homogeneity within each sub-basin and managing the complexity inherent in hydrological modeling. By doing so, it ensured that the modeling approach was both representative of the catchment's diverse characteristics and tractable in terms of computational demands. Secondly, it aligned with the availability of hydrological and meteorological data, a pivotal factor in this study. Each sub-basin could be adequately represented with sufficient data, enabling precise parameterization and calibration of the Hec-HMS model. Furthermore, this reflected practical considerations, including resource constraints and computational efficiency, which were vital for conducting a comprehensive study. The delineated watershed was preprocessed with ArcGIS, a spatial analytical application, in order to extract topographical data. The appropriate coordinate system, or WGS 43 N, was assigned to the watershed. The catchment's dimensions, stream alignments, and basin characteristics including river slope and length were calculated. On the basis of physical characteristics, flow buildup, flow pattern, and areas that were convenient for evaluation, the Khanpur Dam basin was separated into five sub-basins.

Then, for hydrological modeling, the divided basin was loaded into the HEC-HMS model, which was created by the U.S. Army Corps of Engineers as a frequently used piece of software. HEC-HMS is a model for hydrological simulation and evaluation of watershed networks, which allows scientists and water scientists to model and foresee the occurrence of complex hydrological phenomena like precipitation, runoff, evapotranspiration, and streamflow. Owing to its intuitive interface and broad spectrum of features, HEC-HMS modeling makes it possible to create realistic hydrological simulations by selecting catchment variables, patterns of precipitation, land utilization, and soil qualities. The SCS curve number approach, unit hydrographs, and Muskingum–Cunge routing are only a few of the runoff and streamflow routing techniques included in the program. The study of various hydrological scenarios is made easier by using the HEC-HMS model to assist with flood predictions, water resource planning, flood-plain management.

Along with the regular inflows into the reservoir, daily rainfall and temperature statistics for the Khanpur Dam, Murree Station, and the Islamabad (zero point) site were added as well. The settings of the model were meticulously adjusted, and the result was flawless predictions that were compared with values that had been actually obtained. First, the system was calibrated for every year from 2016 through 2018. The verification phase of results was conducted using identical criteria. The results validation step utilized the same parameters. Validation occurred in the years 2019 and 2020.

3.2.4. Model Efficacy Assessment

The efficiency of the HEC-HMS framework was evaluated by employing appraisal indicators for the percent bias (PBIAS), coefficient of determination (R^2), root mean square error (RMSE), and Nash–Sutcliffe efficiency (NSE) [28]. R^2 values which range from -1 to 1 suggest better simulation performances at higher levels. NSE values can vary from 0 to 1, with values over 0.50 considered to be suitable. More simulated errors are indicated by greater numbers [29,44]. The PBAIS should have readings between -15% and +15, according to experts [30]. The mathematical formulas involving R^2, NSE, and RMSE were as follows:

$$\mathrm{R}^2 = \frac{\left[\sum\left(Q_m - \overline{Q_m}\right)\left(Q_s - \overline{Q_s}\right)\right]^2}{\sum\left(Q_m - \overline{Q_m}\right)^2 \sum\left(Q_s - \overline{Q_s}\right)^2} \tag{1}$$

$$\mathrm{NSE} = 1 - \frac{\sum\left(Q_m - \overline{Q_s}\right)^2}{\sum\left(Q_m - \overline{Q_m}\right)^2} \tag{2}$$

$$\text{RMSE} = \sqrt{\frac{\sum_{i=1}^{n}(Q_m - Q_s)^2}{n}} \tag{3}$$

where Q_s, Q_m, $\overline{Q_m}$, and $\overline{Q_s}$ stand for forecasted discharge, calculated discharge, average calculated discharge, and average forecasted discharge, respectively.

3.3. Land Cover Scenarios and Verification of Land Cover Forecasting

Prospective and historical trends of land cover were also investigated in the present research. For the periods between 1995, 2010, 2015, 2018, and 2021, land cover images were produced using Landsat images. After that, areas were marked to determine how every group had changed throughout that particular period. The creation of projected land cover images enabled trend evaluation and hydrological model input, which considered both future climatic circumstances and future land cover conditions. Future land cover maps were simulated using TerrSet's integrated Land Change Modeler (LCM). The land cover conditions for 2040, 2070, and 2100 were predicted in the current study using integrated Markov and CA (CA Markov). The model was executed in two stages using Markov and CA Markov.

3.3.1. Markov Chain Analysis (MCA)

A method of predicting shift forecasting is MCA, which is a general, multimodal stochastic mathematical technique. Prospective pattern forecasts are generated by using past information. If a region is broken down into an assortment of cells, all of which reflect a certain use of land at certain times, MCA estimates the probability that every cell will shift from a single LULC class to a different one in a particular period time frame based on information collected over time frames. The term "transition probability" refers to the likelihood that a condition will change. The shift matrix created by MCA includes the expected pixel alterations and the likelihood that a particular land cover category will switch to the next category [44,45]. As shown below, a Markov shift matrix P can be written as:

$$\left\|P_{ij}\right\| = \left\|\begin{matrix} P_{1,1} & P_{1,2} & P_{1,N} \\ P_{2,1} & P_{2,2} & P_{2,N} \\ P_{N,1} & P_{N,2} & P_{N,N} \end{matrix}\right\| \left(0 \leq \mathrm{P_{ij}} \leq 1\right) \tag{4}$$

where $\mathrm{P_{ij}}$ is the first and second time period types of land cover and P is the likelihood that type 1 land cover will change to type 2 land cover. A set of conditional probability pictures, often referred to as transitional potential maps, emerge after a certain number of time units. These graphics show the chance of each form of land cover appearing at each pixel. The reasons for land cover alterations are not included in a Markov evaluation. A Markov evaluation also has a serious problem with geography since it is spatially insensitive. Therefore, cellular automata were utilized to provide a spatial component to the modeling process.

3.3.2. CA MARKOV

The cellular automata and CA MARKOV-embedded component from the TerrSet program was employed to predict upcoming LULC scenarios. The land cover forecasting framework called CA MARKOV combines cellular automata, Markov chain, multi criteria, and multi-objective land allocation (MOLA) to improve spatial proximity along with data on the anticipated geographic distribution of changes in the Markov Chain assessment. The method works in the following way: The changing regions' data contain the anticipated amount of land cover change from each current division to each of the other groups, following a time frame based on a Markov Chain examination of two previous LULC images. The change simulation is launched using the original land cover image, while the Markov Chain analysis is conducted using subsequent land cover images. To assess each pixel's intrinsic eligibility for each form of land cover, appropriateness maps or transition potential maps are employed [44]. A contiguity filter often downweighs the appropriateness preferring continuous acceptable regions rather than pixels that exceed already existing sections of a category (as of this repetition).

4. Results

4.1. Downscaling of Projected Climate Data

In order to downscale future climate data, a GCM and an appropriate bias correction approach have to be chosen.

4.1.1. Selection of the GCM

For forecasting climate, four different models were obtained for the SSP2 and SSP5 situations. The highest performing of the four GCMs was selected. Table 1 displays the names and other details of the GCM simulations that were obtained and evaluated.

Table 1. Characteristics of the GCM models chosen for the present study.

No.	Model Name	Institute	Nominal Resolution
1	BCCCSM2-MR	Beijing Climate Centre, Beijing, China	1000 km
2	MPI-ESM1-2-HR	Max Planck Institute for Meteorology (Germany)	100 km
3	CMCC-ESM2	Euro-Mediterranean Centre on Climate Change Coupled Climate Model, Italy	100 km
4	CanESM5	Canadian Centre for Climate Modeling and Analysis, Victoria, Canada	250 km

Depending on the needs of a study, a GCM is selected based on the following four primary criteria: (1) resolution, (2) accessible data, (3) prior studies, and (4) degree of performance indicator.

The efficiency of the model is evaluated using performance metrics like the coefficient of determination (R^2) and both past GCM measurements and actual grounded data, as well as the root mean square error (RMSE). Tables 2–4 show how four distinct CMIP6 GCMs performed at the Khanpur Dam stations.

Table 2. GCM models' accuracies for modeling precipitation.

Model	R^2	NSE	PBIAS	MAE	RMSE
BCCCSM2-MR	0.07	−0.79	0.63	68.21	103.16
CMCC-ESM2	0.01	−0.52	−0.29	81.10	89.90
MPI-ESM1-2-HR	0.16	0.05	0.21	58.19	74.16
CanESM5	0.09	−0.41	−0.48	87.70	100.37

Table 3. GCM models' capabilities to simulate highest temperature.

Model	R^2	NSE	PBIAS	MAE	RMSE
BCCCSM2-MR	0.19	−1.52	0.32	10.05	10.08
CMCC-ESM2	0.10	−1.72	0.29	9.85	20.43
MPI-ESM1-2-HR	0.28	−0.39	0.04	5.21	7.06
CanESM5	0.12	−1.62	0.26	8.69	14.52

Table 4. GCM models' capabilities to simulate lowest temperature.

Model	R^2	NSE	PBIAS	MAE	RMSE
BCCCSM2-MR	0.12	−0.89	0.42	15.16	17.80
CMCC-ESM2	0.09	−1.47	0.63	19.07	19.06
MPI-ESM1-2-HR	0.26	−0.38	0.17	5.19	8.24
CanESM5	0.11	−0.84	0.29	11.33	16.87

The "MPI-ESM1" model was chosen as the climate model for evaluating future climatic trends of the research region because it had comparably better R^2, NSE, and RMSE values than the other models for rainfall, highest temperature, and minimum temperature, as listed in Tables 2–4 above. This study evaluated climate forecasts for the time period 2016–2100, including precipitation as well as minimum and maximum temperatures, for the MPI–ESM1 model for both shared socioeconomic pathways (i.e., SSP2 and SSP5). Applying the hydrological simulation software CMhyd-2016 with inputs from the climate model, the datasets were bias corrected.

4.1.2. Selection of Bias Correction Approaches

GCMs produce positive outcomes when modeling the more extensive observations of data, but when studied at the basin level, they still show significant bias [24]. The aim of a bias adjustment strategy is to employ a certain corrective component for modifying a predicted time series variable's mean, variance, and/or quintile so that adjusted modeled time series match factors that are observed. To try to determine the optimal downscaling methodology for the acquired GCM information, five varying rainfall adjustment strategies (Table 5) and four distinct temperature adjustment procedures (Table 5) were explored. The Khanpur Dam catchment station's temperature and precipitation were corrected using all available approaches (Tables 6 and 7), and then the effectiveness of the corrections were assessed, as demonstrated in Table 8 via time series analytics.

Table 5. Approaches for bias corrections for temperature and precipitation.

Bias Correction for Precipitation	Bias Correction for Temperature
• Linear scaling (LS) • Local intensity scaling (LOCI) • Power transformation (PT) • Distribution mapping (DM) • Delta change (DC)	• Linear scaling (LS) • Variance scaling (VS) • Distribution mapping (DM) • Delta change (DC)

Table 6. Comparison of precipitation downscaling methods.

Model	Method	R^2	NSE	PBIAS	MAE	RMSE
MPI-ESM1	Raw (model simulated historical)	0.17	0.04	0.22	60.89	86.28
	Delta change	0.68	0.60	0.10	31.72	46.83
	Distribution mapping	0.71	0.73	0.09	28.80	40.02
	Linear scaling	0.65	0.57	0.12	42.61	60.19
	Power transformation	0.79	0.78	0.04	19.42	29.44
	Local intensity scaling	0.66	0.58	0.11	36.27	53.47

Table 7. Comparison of highest and lowest temperature downscaling methods.

Model	Method	R^2	NSE	PBIAS	MAE	RMSE
MPI-ESM1	Maximum Temperature					
	Raw (model simulated historical)	0.26	−0.58	0.06	7.62	9.00
	Delta change	0.68	0.36	0.20	3.69	5.72
	Distribution mapping	0.86	0.72	0.02	2.56	3.76
	Linear scaling	0.78	0.56	0.10	2.96	4.73
	Variance scaling	0.75	0.48	0.16	3.32	5.15
	Minimum Temperature					
	Raw (model simulated historical)	0.23	−0.55	0.26	7.28	9.40
	Delta change	0.64	0.29	0.18	3.58	6.40
	Distribution mapping	0.88	0.76	0.05	2.11	3.70
	Linear scaling	0.77	0.53	0.14	3.15	5.20
	Variance scaling	0.80	0.64	0.10	2.85	4.56

Table 8. Outline of shift in hydrology under climate change.

Climate Scenarios	Precipitation	Maximum Temperature	Minimum Temperature	Flows (Current Land Use Land Cover Future Climate)	Flows (Future Land Cover and Present Climate Change)
	% change	% change	% change	% change	% change
SSP2	21	4.9	13.1	16.9	19.8
SSP5	28	9.1	24.1	21.2	25.1

The estimated output metrics showed that each bias adjustment enhanced the initial GCM simulations. Overall, the monthly mean values of both temperature and precipitation can be corrected using any of the bias correction techniques. Based on their variability range and capacity to improve the fit of raw GCM median to data, for temperature, "distribution mapping" and, for precipitation, the "power transformation" delivered the best results.

4.2. Expected Changes in Precipitation and Temperature

Following selection of the GCM and downscaling approaches for temperature (max and min) and rainfall, the predicted data were scaled down for the twenty-first century. Two databases were produced for expected temperature and precipitation, i.e., a historical dataset from 1990 to 2015 and a projected database from 2016 to 2100.

4.2.1. Forecast for Mean Maximum Temperature

Up to the end of the twenty-first century, it is anticipated that the maximum temperature in the Khanpur Dam catchment area will climb from 22.6 °C within the initial period (1990–2015), with increases of 4.9% and 9.1% under SSP2 and SSP5, respectively. For a periodic analysis of this temperature shift, the months of the year are divided into four different seasons as follows: winter months are November, December, and January; spring months are February, March, and April; the autumn months are August, September, and October; the summer months are May, June, and July (Table 8).

As shown in Figure 3, the analysis of seasonal variation reveals that each of the four seasons had increased peak temperatures. Figure 3 shows that the peak winter temperatures increase from 14.06 °C to 14.86 °C and to 15.63 °C under SSP2 and SSP5, respectively. Under SSP2 and SSP5, the peak summer temperatures increase from 24.7 °C to 25.59 °C and to 26.36 °C; however, the peak autumn temperatures increase from 21.91 °C to 22.83 °C and to 23.6 °C, respectively. The maximum temperatures in springtime increased under SSP2 and SSP5, respectively, from 16.71 °C to 17.4 °C and to 18.17 °C. Climate change has played a significant role in increasing the maximum temperature within the Khanpur Dam catchment area. One of the primary mechanisms behind this phenomenon is overall warming of the Earth's climate due to an increased concentration of greenhouse gases, such as carbon dioxide, in the atmosphere. These gases trap heat from the sun, leading to a general rise in global temperatures. In the specific context of the Khanpur Dam catchment area, this global warming effect translates into hotter summers and prolonged heatwaves. Additionally, changes in regional climate patterns, such as altered precipitation and increased aridity, can exacerbate the warming trend. As a result, the higher temperatures not only directly influence the local climate but also contribute to increased evaporation rates from the dam's reservoir, potentially affecting water availability and overall ecosystem health. Understanding these temperature changes and their drivers is essential for effective climate adaptation and water resource management in the region [45,46].

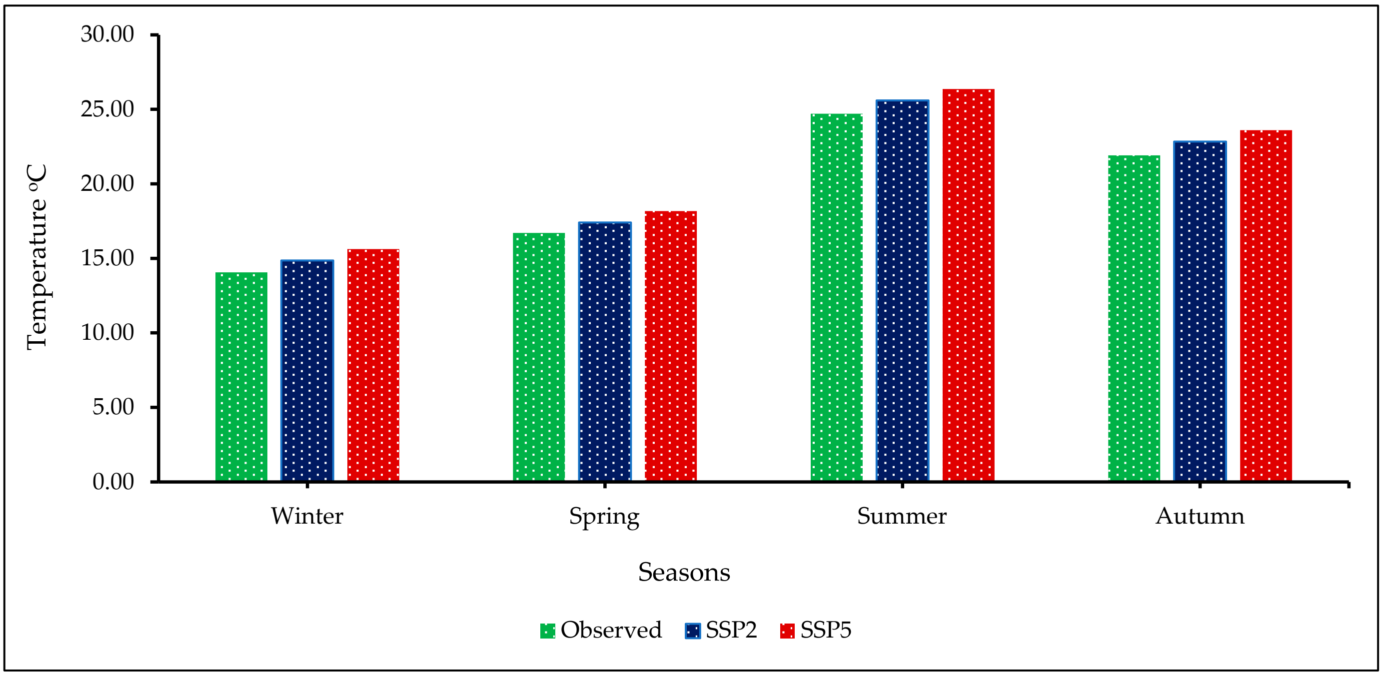

Figure 3. Comparison of the Khanpur catchment area's seasonal maximum temperature during climate change.

4.2.2. Forecasting of Mean Minimum Temperature

Up to end of the twenty-first century, it is expected that tmin in the catchment area of the Khanpur Dam would increase from 8.6 °C during the initial timeline (1990–2015) to 9.7 °C for SSP2 and 10.6 °C for SSP5. The months of the year, divided into four seasons (winter being November, December, and January), were utilized to study this evolution from a seasonal viewpoint. While August, September, and October are regarded as autumn months, May, June, and July are known as summer months.

The study of seasonal variation (Figure 4) shows that the minimum temperature increases over the four different schedules. Figure 4 shows that the minimum winter temperature increases from 3.6 °C to 4.4 °C and to 5.2 °C for SSP2 and SSP5, respectively. For SSP2 and SSP5, the maximum summer temperatures increase from 15.7 °C to 16.5 °C and to 17.2 °C, respectively, while the maximum autumn temperatures increase from 10.7 °C to 11.5 °C and to 12.2 °C, respectively. The peak springtime temperatures increase under SSP2 and SSP5, from 7.1 °C to 7.9 °C and to 8.6 °C, respectively. Climate change has led to an increase in the minimum temperature throughout the year within the Khanpur Dam catchment area. This phenomenon is primarily attributed to the global warming trend resulting from the accumulation of greenhouse gases in the atmosphere. Elevated levels of greenhouse gases trap heat, preventing it from escaping into space, and consequently, the planet experiences higher temperatures. In the context of the Khanpur Dam catchment area, this translates into milder and warmer winters and nights. The warmer minimum temperatures are not limited to a particular season but persist year round. Climate change can disrupt traditional temperature patterns, affecting ecosystems and agriculture. Additionally, altered temperature regimes can influence precipitation patterns, exacerbating water stress and further impacting the local environment and water resources in the region. Understanding and addressing these shifts in minimum temperatures is crucial for climate adaptation and sustainable resource management in the Khanpur Dam catchment area and similar areas affected by climate change.

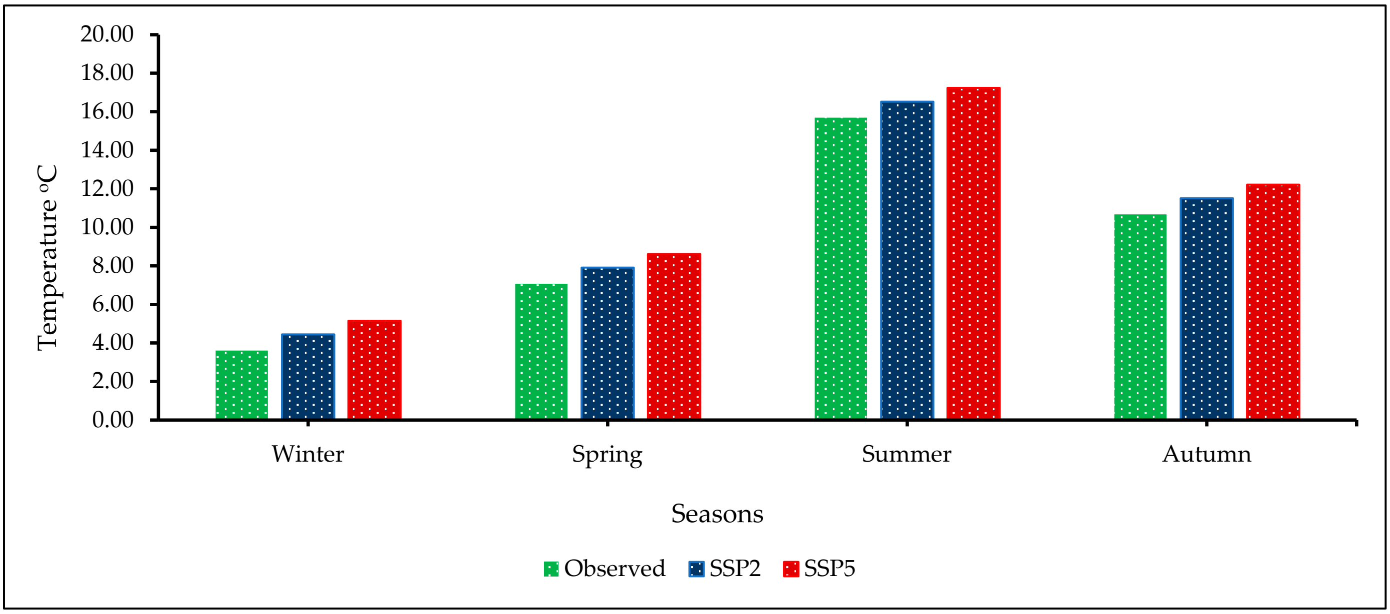

Figure 4. Comparison of seasonal tmin in the Khanpur catchment area under climate change.

4.2.3. Precipitation Forecasting

Precipitation in the Khanpur Dam basin region is anticipated to rise by 21% and 28% by the end of the twenty-first century, between 1532.7 mm in the original timeframe (1990–2015) to 1854.5 mm and to 1961.8 mm, under SSP2 and SSP5, respectively. The months of the year, divided into four seasons (spring is February, March, and April, while winter is November, December, and January), were utilized to study its evolution from a seasonal viewpoint. While August, September, and October are regarded as autumn months, May, June, and July are considered to be summer months.

For summer, winter, and fall, we saw a spike in rainfall, while in spring, there was a decrease, according to the study of seasonal change shown in Figure 5. Winter precipitation increased under SSP2 and SSP5 from 45.3 mm to 47 mm and to 54 mm, respectively. Summer and fall rainfall increased more noticeably than winter precipitation, but otherwise followed a similar pattern. For instance, rainfall increased from 157.3 mm to 228.5 mm in the summer and from 222.9 mm to 252.5 mm in the autumn under SSP2, whereas under SSP5, it increased from 170.8 mm to 236.7 mm in the summer and from 252.5 mm to 252.5 mm in the autumn. In contrast, it is anticipated that, for SSP2 and SSP5, the amount of rainfall in the Khanpur Dam basin region, in spring, will drop from 106.4 mm to 93.5 mm and to 88 mm, respectively. Climate change has had a multifaceted impact on the precipitation patterns within the Khanpur Dam catchment area throughout the seasons. The observed increases in precipitation during winter, summer, and autumn can be attributed to several factors. Warmer temperatures associated with climate change can lead to greater evaporation rates, which, in turn, can increase moisture in the atmosphere. This increased moisture content can contribute to heavier rainfall during these seasons. Additionally, altered atmospheric circulation patterns due to climate change can result in changes in the paths and intensity of storms, further enhancing precipitation.

Conversely, the decrease in precipitation in spring is likely influenced by the same factors but in a different manner. Warming temperatures in spring can lead to earlier snowmelt in mountainous regions surrounding the catchment area. This premature snowmelt can reduce the availability of moisture during the spring months when it is traditionally expected, leading to drier conditions. The shift in precipitation patterns, with increased rainfall in other seasons and decreased spring precipitation, poses challenges for water resource management, agriculture, and ecosystems within the Khanpur Dam catchment area. Adaptation strategies and long-term planning are crucial to address these changing precipitation dynamics and their implications for the region.

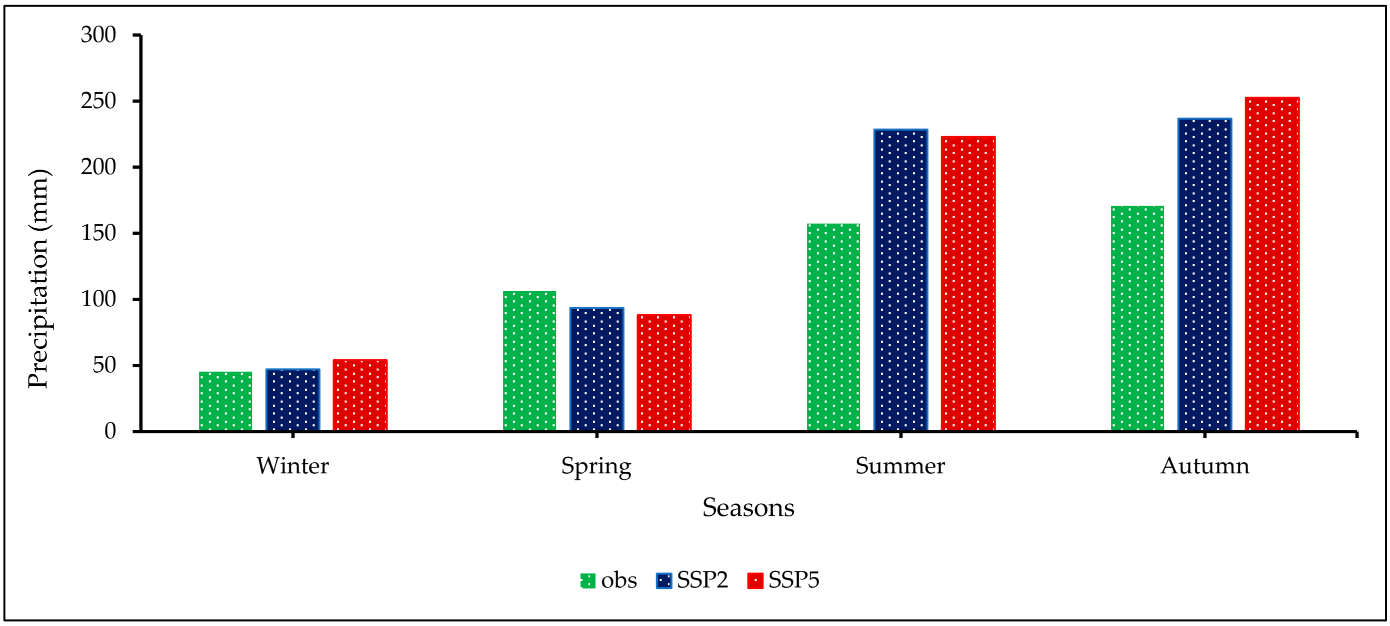

Figure 5. Seasonal precipitation in the Khanpur catchment area under climate change comparison.

4.3. Land Cover Change Trends

The mosaicked Landsat 2000, 2013, and 2023 images were categorized unsupervised using ArcGIS's image classification tool. Figure 6 displays the categorized images of the study site. Seven categories were created from the images as follows: vegetation, flooded vegetation, barren ground, water bodies, shrubs and scrub, and built-up areas.

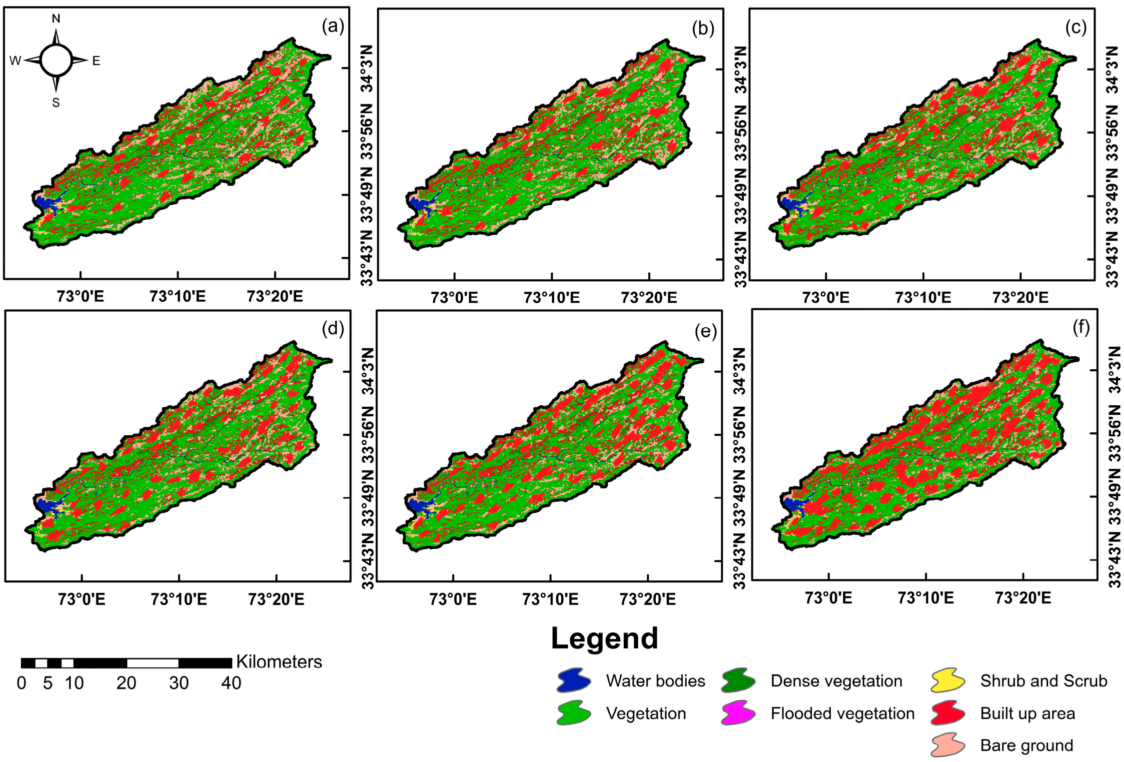

Figure 6. Land use and Future maps: (**a**) 2000, (**b**) 2010, (**c**) 2020, (**d**) 2030, (**e**) 2070 and (**f**) 2100, accordingly.

Using the embedded Land Change Modeler in TerrSet, land cover maps for the years 2030, 2070, and 2100 were created. In 1987, Prof. J. Ronald of Clark University created TerrSet, a Geospatial Monitoring and Modeling System comprised of tools for studying image time series. Future land cover is simulated using the cellular automata-Markov chain model (CA-MCM).

Figure 6 shows the projected land cover maps for the research region. The results indicate that, in the watershed of the Khanpur Dam, the areas of water bodies, vegetation, bare land, dense vegetation, flooded vegetation, and scrub decreased by 3.6%, 6.8%, 5.5%, 4.6%, and 3.9%, respectively, between 2000 and 2100. Even though the built-up area increased by 28.9%, this is still a considerable growth. Figure 7 depicts this shift in land cover classifications. The increase in the built-up area within the Khanpur Dam catchment area can be attributed to various socioeconomic factors, including population growth, urbanization, and infrastructure development. As the local population continues to expand, there is a rising demand for residential, commercial, and industrial areas, resulting in the conversion of natural landscapes into built-up environments. This urban expansion often leads to the transformation of water bodies, vegetation, bare land, dense vegetation, flooded vegetation, and scrub into paved surfaces and structures. Additionally, factors like increased agricultural activities and deforestation can further contribute to land use changes. Simultaneous decreases in the natural and semi-natural land cover types underscore the complex interplay between human activities and environmental dynamics, emphasizing the need for sustainable land use planning and conservation efforts to mitigate the ecological and hydrological impacts of these transformations.

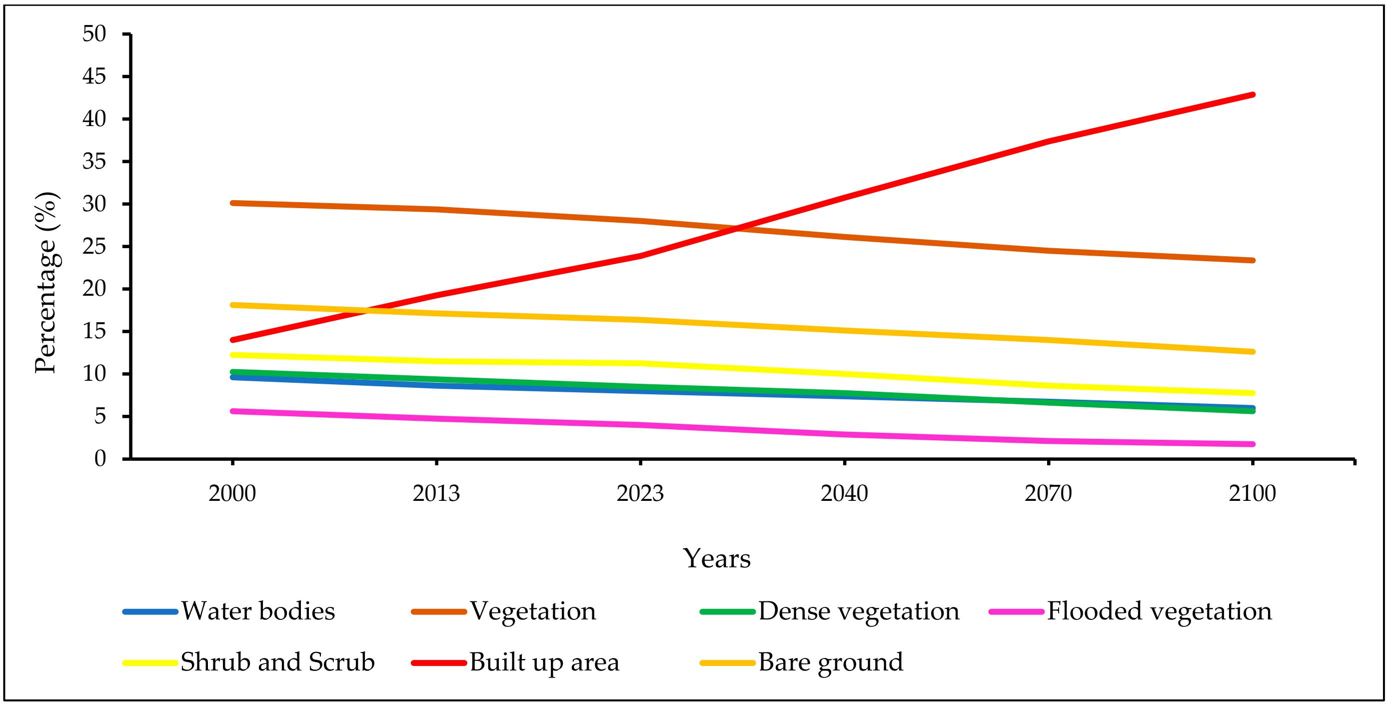

Figure 7. Calculations of land cover areas and their trends over time.

4.4. Calibration and Validation of the Hydrological Model

The HEC-HMS model has been deployed by many academics and industry professionals for hydrological modeling. For the years 2016–2100, hydrological modeling of the Khanpur Dam basin area was conducted to analyze the effect of CC and LULC on the catchment area's water availability. Through this procedure, the model was calibrated and validated. In the context of utilizing a Hydrologic Engineering Center's Hydrologic Modeling System (HEC-HMS) model for hydrological modeling, it becomes evident that a thorough grasp of essential components is indispensable for a precise depiction of the intricate hydrological cycle. These pivotal elements encompass loss mechanisms that address water diminishment due to factors such as evaporation and transpiration; transformation processes, covering shifts in water states like snowmelt and ice melt; base flow, signifying the consistent groundwater-fed contributions to river and streamflow; and channel processes that dictate the hydraulic and geomorphic characteristics of watercourses. The incorporation and accurate portrayal of these elements within the HEC-HMS model is crucial, as it fosters a more robust and meticulous simulation of hydrological processes, facilitating comprehensive evaluations of water movement within the specified study area.

In the conducted hydrological modeling, a combination of methods was employed to effectively represent key components of the hydrological cycle. To account for loss processes, both the deficit and constant methods were utilized. The deficit method enabled the assessment of water diminishment caused by phenomena such as evaporation and transpiration, offering a comprehensive understanding of the overall water balance. Simultaneously, the constant method provided valuable insights into steady-state losses, shedding light on the persistent nature of these reductions over time.

In addressing transformation processes, the Clark unit hydrograph method was applied. Rooted in fundamental rainfall-runoff transformation principles, this method allowed for accurate representation of changes in water states, particularly those resulting from snowmelt and ice melt. Its ability to capture the temporal dynamics of runoff contributed significantly to the precision of the hydrological model. Additionally, to model the base flow component, the recession method was utilized. This approach provided nuanced insights into the gradual, groundwater-derived contributions to river and streamflow, ensuring a comprehensive representation of base flow dynamics within the hydrological cycle.

4.4.1. Deficit and Constant Method

The "deficit and constant" method, employed as a quasi-continuous model to calculate precipitation loss, operates with the characteristic feature of initial loss recovery following extended dry periods devoid of rainfall. This method utilizes a single layer to account for ongoing changes in moisture content. In accordance with the HEC-HMS user's manual [47], the "deficit and constant" method is typically recommended for use in conjunction with the "canopy" method. The "canopy" method leverages potential evapotranspiration, as determined by meteorological models, to extract water from the soil and represents the influence of vegetation in the landscape. The soil layer tends to desiccate between storm events as the canopy withdraws moisture, though it is worth noting that soil water extraction is only realized when employing a 25-canopy method. Additionally, the "surface" method, in which water accumulates within depression surface storage, can be employed as an alternative approach. In the "deficit and constant" method, percolation transpires when the soil layer attains saturation. The key parameters that are integral to this approach include initial deficit (measured in mm/day), maximum deficit (measured in mm/day), constant rate (measured in mm/day), and imperviousness percentage (%). The initial deficit represents the quantity of water necessary to fill the soil layer up to its maximum storage capacity, while the maximum deficit, quantified as depth, delineates the soil layer's water-holding capacity. The constant rate defines the percolation rate when the soil layer reaches saturation. By specifying the impervious area percentage, the contribution of impervious surfaces to the overall loss calculations is duly excluded.

4.4.2. Clark Unit Hydrograph

The Clark unit hydrograph method was applied, which leverages the concept of an instantaneous unit hydrograph to route excess precipitation toward the sub-basin outlet. In this approach, an instantaneous unit hydrograph is derived by immediately applying a unit depth (e.g., one inch) of excess precipitation over the entire watershed [48]. This method effectively captures two crucial processes involved in the transformation of excess precipitation into runoff: (1) translation, or movement, of excess precipitation from its origin throughout the watershed to the outlet, and (2) attenuation, or reduction, in discharge magnitude as excess precipitation is temporarily stored within the watershed (U.S. Army Corps of Engineers) [49]. These processes are explicitly integrated to estimate the hydrograph at the outlet of the watershed. Initially, runoff is translated to the watershed outlet with a delay, devoid of attenuation. Subsequently, attenuation is introduced at the watershed outlet. Within this method, three parameters are employed:

- The time of concentration (Tc), which is equivalent to the duration it takes for excess precipitation to travel from the hydraulically most remote point of the watershed to the outlet.
- The watershed storage coefficient (R), corresponding to the attenuation attributed to storage effects across the watershed [50].
- The time-area histogram, which depicts the portion of the watershed area contributing to flow at the outlet in relation to time. This method is well-established, thoroughly documented, and straightforward to set up and utilize. Additionally, it allows for regionalization of parameters, their correlation with measurable basin characteristics, and variability with excess precipitation rates. These attributes are particularly valuable for applications in dam safety studies. A prior study had formulated regional regression equations to estimate Clark unit hydrograph parameters across California, as part of a Memorandum of Agreement with DSOD (U.S. Army Corps of Engineers) [51].

4.4.3. Recession

The "recession" base flow method was employed for basins characterized by an exponential decline in channel flow following a storm event. This method is designed for both event-based and continuous simulations and entails the selection of three key parameters: the "initial type", the "recession constant", and the "threshold type". The "initial type" offers two options, which are the initial discharge and the initial discharge per area. The choice between these two options depends on the availability of observed flow records. If such records are accessible, the initial discharge method is applied; otherwise, the initial discharge per area is utilized. In cases where the latter method is employed, estimations can be based on general guidelines used for assessing basin yield to determine the initial flow. The rate at which base flow recedes, represented by the recession constant, determines the ratio of base flow at day t to the base flow at the preceding day $(t - 1)$. To reset the base flow, either the ratio to peak or threshold flow methods can be adopted, depending on the preference and requirements of the analysis.

At the location of the Khanpur Dam, the Haro River was utilized for model calibration and validation. Finding the perfect combination of parameters that closely matches the observed and simulated discharge is a necessary step in the calibration process. In our study, we adopted a trial-and-error procedure as a fundamental component of the calibration process. This method involves systematically adjusting various model parameters, such as initial loss coefficients, curve number values, and channel routing parameters, through a series of iterations. The goal is to fine tune these parameters until the model's simulated results align closely with the observed data. During each iteration, parameter values are modified, and the model is rerun to assess the impact of these adjustments on its performance. This iterative approach allows us to identify the parameter combinations that best represent the physical processes of the watershed under study. The trial-and-error procedure acknowledges the complexity of hydrological systems and the inherent uncertainties in modeling them. It ensures that the model's output is a more accurate reflection of the real-world hydrological processes, ultimately leading to a higher degree of confidence in the model's predictive capabilities. While we recognize that a more detailed explanation of this procedure is necessary for clarity, the trial-and-error calibration method remains a fundamental and widely accepted approach in hydrological modeling, particularly in cases where complex processes and numerous parameters need to be considered for model calibration. All the values presented in Table 9 have been meticulously obtained through this iterative "trial-and-error" procedure during the calibration phase of our study. The model is calibrated from 2016 to 2018, and then validated from 2019 to 2020. The calibration's input variables are listed in Table 9.

Table 9. Variable values for calibration and validation.

Sub-Basin	Loss Method			Transform Method		Base Flow Method
	Initial Deficit (mm)	Max Deficit (mm)	Constant Rate (mm/h)	Time of Concentration (h)	Storage Coefficient (h)	Recession Constant
1	13	27	2.5	4	8	0.85
2	13	27	2.4	4	9	0.85
3	13	27	1.7	2.8	5	0.85
4	13	27	1.8	2.8	5	0.85
5	13	27	1.6	2.4	3	0.85

Within HEC-HMS modeling for the Khanpur Dam basin, we acknowledge the inherent uncertainty in estimating model parameters. In addressing this uncertainty, we consider the variability in critical parameters, including initial deficit, maximum deficit, constant rate, time of concentration, storage coefficient, and recession constant, all of which significantly influence the model's outcomes. The uncertainty analysis begins with a systematic examination of the sources of variability within these parameters. For instance, the initial deficit parameter introduces uncertainty due to its influence on the quantity of water required to reach the soil layer's maximum storage capacity during rainfall events. Similarly, the maximum deficit parameter's uncertainty stems from variations in the depth of the soil layer's water-holding capacity and its implications for hydrological processes. To mitigate this uncertainty, our study incorporated a sensitivity analysis to assess how parameter variations affected the model's performance. The sensitivity analysis allowed us to identify which parameters had the most substantial impact on the model's predictive accuracy. This process involved systematically adjusting these parameters and observing the resulting changes in the model's outcomes. Through the sensitivity analysis, we could recognize the parameters, such as constant rate, which play vital roles in determining the percolation rate when the soil layer reaches saturation, and their influence on the model's ability to accurately simulate hydrological processes.

While our study does not explicitly address the concept of equifinality, the sensitivity analysis and the fine tuning of these parameters play a crucial role in managing parameter uncertainty. By systematically assessing the influence of these parameters on the model's performance, we enhance the model's reliability and credibility. This approach enables us to provide accurate insights into the implications of climate change and land use alterations on water availability within the Khanpur Dam basin, while considering the associated uncertainty in parameter estimation. The model successfully replicated the daily and monthly discharges. When it comes to reproducing the low, medium, and peak flows, the model is reliable. Figures 8 and 9 show, respectively, how the Haro River calibration and validation were done. The HEC-HMS model's calibration and validation revealed an acceptable level of agreement between the observed and anticipated discharges. Table 10 gives the calibration and validation values for the Nash–Sutcliffe coefficient, RMSE, and determination R^2.

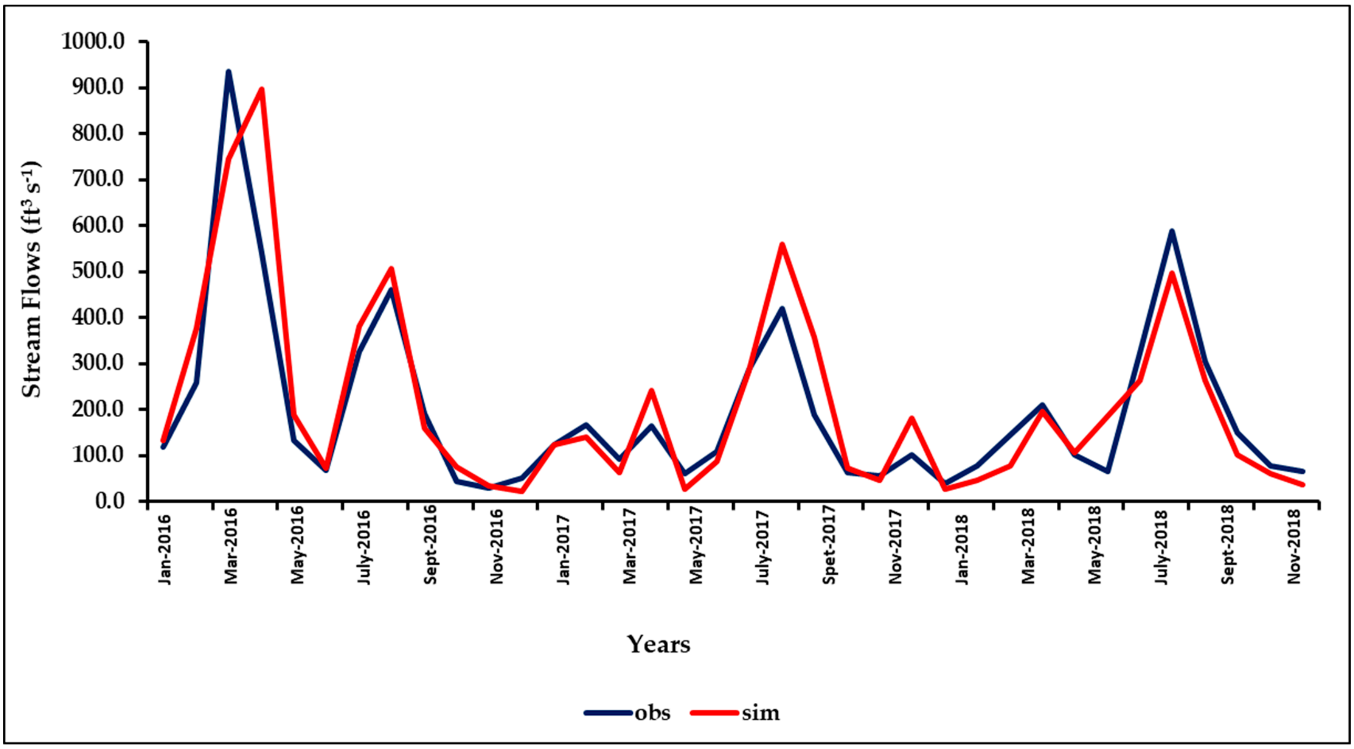

Figure 8. Flows during the 2016–2018 calibration period, simulated and observed.

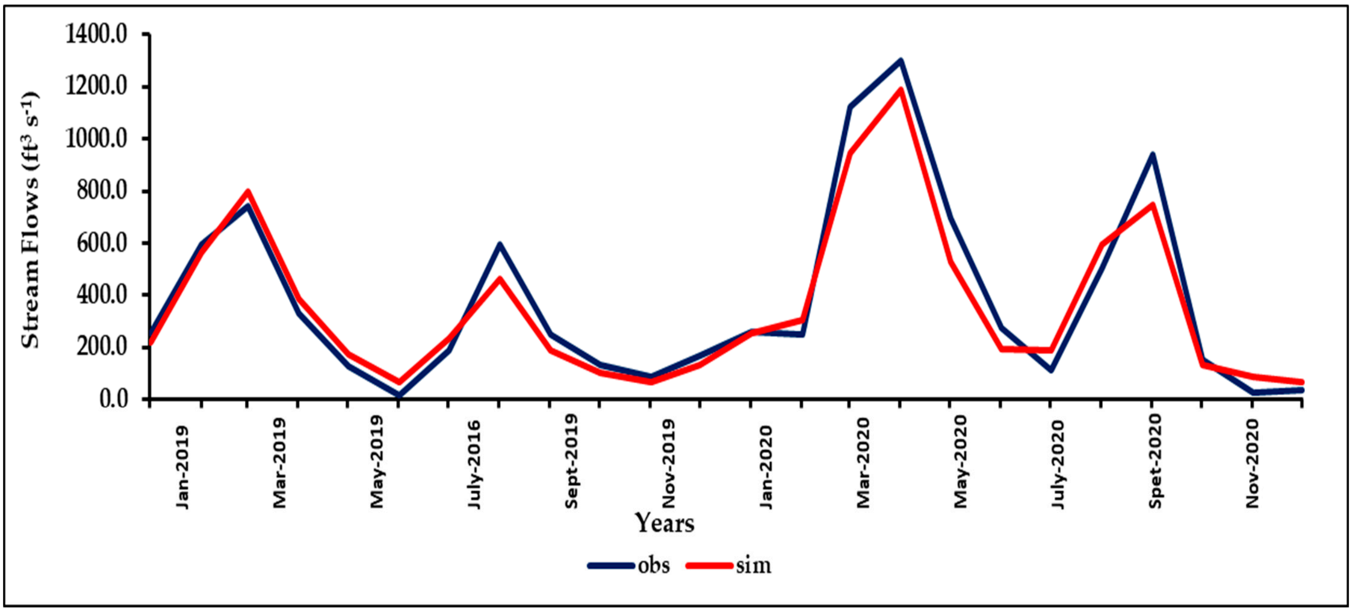

Figure 9. Flows for the 2019–2020 validation period, simulated and observed.

Table 10. Statistics for the calibration and validation of the hydrological model for the month.

Parameters	Calibration	Validation
NSE	0.82	0.83
R^2	0.81	0.79
RMSE	1.98	2.4

4.5. Effect of Forecasted Climate on Flows

Once the model was calibrated and confirmed, this configuration was used to predict future flows on a yearly schedule from 2016 to 2100. Two simulations' future flows were analyzed.

Hydrological response to expected climate and present land cover and hydrological response under current climate and projected land cover are two hypothetical situations.

Scenario A evaluates the hydrological response considering the expected climate and present land cover.

By the end of the century, inflows according to climate change were forecasted employing calibrated models. The tmax rose with SSP2 and SSP5, respectively, by 4.9% and 9.1%, the tmin by 13.1% to 24.1%, and the precipitation grew by 21% and 28%. In Table 11, it is shown that with SSP2 and SSP5, flow rates will rise from 261.8 cusecs in the beginning duration (1990–2015) to 306 cusecs and 317.3 cusecs, respectively, in the foreseeable time span (2016–2100). In the present-day scenario with unchanging land cover, the variations in temperature and rainfall were entered into the verified HEC-HMS simulation.

Table 11. Change in flows by percentage at the Khanpur Dam in Scenario A (i.e., forecasted climate and present land use).

Climate Scenarios	**Flows (Current Land Use Land Cover Future Climate) (2016–2100)**	
	cusecs	% change
Observed	261.8	-
SSP2	306	16.9
SSP5	317.3	21.2

Figure 10 relates average monthly inflows of the initial era (1990–2015) to inflows throughout the future time span for SSP2 and SSP5 assumptions to investigate historical trends in the average month inflows in the Khanpur Dam basin. The SSPs predict a spike in inflow during the full year.

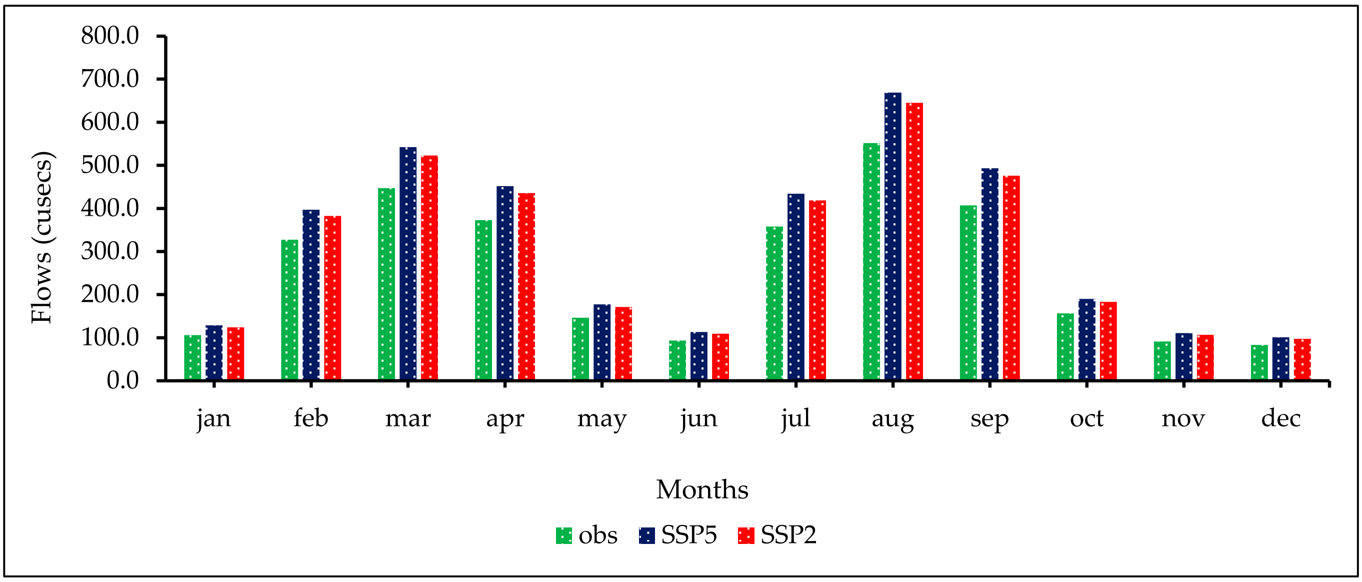

Figure 10. Khanpur Dam inflow comparison for Scenario A (i.e., forecasted climate and current land use).

Scenario B: hydrological response in light of future land cover and future climate.

Then, the calibrated method was utilized for predicting flows considering forecasted temperature and anticipated LULC transition once flows were anticipated of anticipated climate and current LULC. Land cover trends show that the Khanpur Dam basin's built-up area increased by 28.9% between 2000 and 2100. Given that, as a whole, the metropolitan region is 70% impermeable and the remaining 20% is made up of houses, lawns, etc., the transition of industrialization was additionally broadened and added to the model as imperviousness with an index of 0.7. The percentages of various land use groups, such as water bodies, vegetation, bare land, dense vegetation, flooded vegetation, shrubs, and scrub, decreased by 3.6%, 6.8%, 5.5%, 4.6%, and 3.9%, respectively, in the Khanpur Dam catchment area. The shift in land utilization and climate factors acquired throughout the initial era (1990–2015) are subsequently incorporated into the corrected HEC-HMS program with rising impermeability so as to analyze the impacts of development on inflows of the Khanpur Dam. The results show the inflows would increase from 261.8 cusecs during the initial time (1990–2015) to 313.5 cusecs under SSP2 and from 261.8 cusecs during the benchmark era (1990–2015) to 327.6 cusecs under SSP5 (Table 12).

Table 12. Shift of flows as a percentage in Scenario B at the Khanpur Dam (i.e., anticipated climate and future land cover).

	Flows (Future Land Cover and Future Climate) (2016–2100)	
	cusecs	% change
Observed	261.8	-
SSP2	313.5	19.76
SSP5	327.6	25.13

Figure 11 examines the temporal fluctuations in the Khanpur watershed by comparing mean monthly flows throughout the initial timeline (1990–2015) in light of anticipated flows and changing land cover. Flows had a pattern of increasing during the whole year. The increase in flows at the Khanpur Dam under the combined influence of climate change scenarios SSP2 (shared socioeconomic pathway 2) and SSP5 (shared socioeconomic pathway 5) along with land use changes can be attributed to several interconnected factors. Firstly, climate change, as projected under these scenarios, is expected to bring about alterations in precipitation patterns, including an increase in extreme rainfall events. This intensification of rainfall can lead to higher runoff and increased streamflow into the dam, particularly during the monsoon season. Additionally, rising temperatures linked to climate change can accelerate snowmelt in the catchment area's mountainous regions, further contributing to increased flows, particularly in the early spring. Secondly, land use changes driven by human activities can play a pivotal role. Urbanization and deforestation, often associated with SSP2 and SSP5, can lead to changes in the hydrological characteristics of the catchment area. Paved surfaces and impermeable urban landscapes can enhance surface runoff and decrease infiltration, channeling more water directly into the dam. Simultaneously, deforestation reduces the capacity of vegetation to intercept and absorb rainfall, leading to higher runoff rates. These land use changes can collectively amplify the impacts of climate change on flow patterns, resulting in increased flows at the Khanpur Dam.

The combined effects of climate change and land use change on flows at the Khanpur Dam highlight the need for integrated water resource management strategies that consider both environmental and socioeconomic factors. It underscores the importance of adapting to changing hydrological regimes and implementing sustainable land use practices to mitigate potential risks and ensure the availability of water resources in the face of evolving climate and land use scenarios.

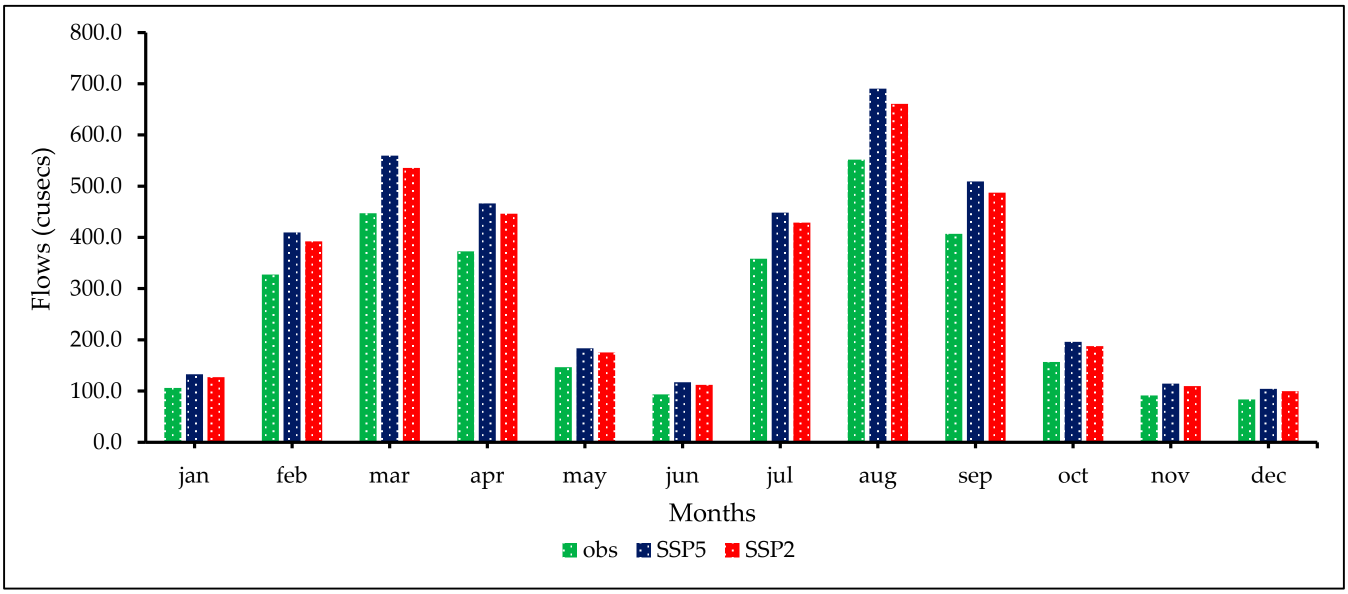

Figure 11. Flow comparison at the Khanpur Dam for Scenario B (i.e., future climate and future land cover).

5. Discussion

Wintertime precipitation is mostly snow, especially in northern regions. According to information on river flow, the highest discharge is observed in July, with an average yearly inflow of 261.8 cusecs as estimated at the Khanpur Dam gauge station [28,29]. Many of the results from the CMIP6 GCMs are viewed as a useful choice for comprehending how climate change impacts river flow patterns [45–49]. The objective of the present investigation was to analyze how anticipated changes in land cover and climate might affect inflows in the Marghalla Hills basin of the Khanpur Dam. To evaluate foreseeable consequences of anticipated LULC and CC, a corrected HEC-HMS hydrological model was employed [52–54]. The downscaled forecasts of temperature and precipitation from the selected GCM (MPI-ESM1-2-HR) were in excellent accordance with forecasts obtained from gauge-based calculations (1990–2015). This could be because the CMIP6 scenarios have significantly better abilities to predict rainfall and temperature in Karakoram, Himalaya, and Hindukush areas [33–36].

The outcomes of the product evaluation of the GCM (MPI-ESM1-2-HR) revealed continued warming on annual and seasonal timescales throughout the basin region of the Khanpur Dam in the twenty-first century, characteristics that are comparable with those in nearby South Asian regions of the Tibetan Plateau [55,56] and Himalaya [33–36,38,39]. The much higher temperatures in the HKH Mountains may be due to regional climate-elevated quantities of greenhouse gases and aerosols [57,58]. On average, it is predicted that there will be more precipitation in the future (2016–2100). Between 2015 and 2100, an increase in the waterways of the Yellow River region was also seen [59]. Precipitation is anticipated to rise across the board in the future, with the summer and fall seeing the largest increases, according to the GCM. These results conflict compared to those from the upper Cruz River watershed and Kelantan River region in Malaysia [60,61]. The seemingly contradictory trend of summer rainfall tending to fall in areas with powerful westward winds (Afghanistan and Iran) was also uncovered by Ozturk et al. [62]. However, seasonal rainfall trends in the studied region mimic those of the Karakoram and Himalayan ranges. According to Babur et al. [46], the Jhelum River watershed of the Himalayan Mountains has experienced growing regular and yearly rainfall patterns. Garee et al. [63] and Pande et al. [64] have predicted that inter-annual and seasonal rainfall would show a stronger tendency for rain to fall over the Karakoram Mountains in the Hunza River valley [65–69]. The observed parallelism may be attributed to the predominance of westerlies circulatory pattern in the Hindukush Himalaya [70–73]. The high level of human-made aerosols in the South Asian environment is a different factor contributing to such analogies in rainfall patterns [74–76].

An examination of the HEC-HMS model's expected flows reveals that, annually, the average flow for the two SSPs (SSP2 and SSP5) is increasing over the course of the forecasted time periods [77–79]. Increases in future flow may be attributed to projected increases in yearly rainfall and global change [80–82]. he anticipated rise in future water flow can be linked to two main factors: the projected increase in annual rainfall and the broader impacts of global environmental changes [83–85]. As climate patterns evolve, leading to shifts in precipitation, regions may experience greater amounts of rainfall annually [86–88]. Additionally, the broader context of global environmental changes, such as alterations in temperature and atmospheric conditions, can influence the hydrological cycle, further contributing to increased water flow in the future [89–91]. These combined factors emphasize the complex interplay between climate and the environment, highlighting the need for proactive water resource management and adaptation strategies to address the changing dynamics of water availability [92–95]. The Indus River and Swat River levels will also increase, according to projections made by Immerzeel et al. [96–98] and Masood et al. [20], respectively.

6. Conclusions

The hydrological behavior of the Khanpur Dam basin to past rainfall was simulated using HEC-HMS modeling. Then, the potential aspect of changing LULC and climate on dam inflows was determined using trained simulation. The Khanpur Dam catchment area was divided into five sub-basins by the HEC-HMS hydrological approach, with distinctive characteristics. To monitor the overall dam basin area, three climatic sites were picked: Murree, Islamabad (zero point), and the Khanpur Dam. For the timelines 2003–2005 and 2006–2007, the simulation was tested and chosen. Following calibration, the model's attributes were modified, and then the calibrated model was employed for affirmation. Comparing expected and actual storage stages, the model showed satisfactory concordance. Then, the CMhyd software employed climate change rainfall forecasts for both shared socioeconomic pathways (SSPs) (SSP2 and SSP5), statistically downscaling data produced from the GCM (MPI-ESM1-2-HR). Upon downscaling, forecasts were included for the calibrated model to identify any repercussions from CC on the Khanpur Dam. This study was carried out for the baseline (1990–2015) and (2016–2100), which covered the present century. A few takeaways of the study are as follows:

- Since 2016, the annual minimum, maximum, and mean temperatures and precipitation in the Khanpur Dam basin have been rising gradually compared to those of the reference period (1990–2015). The increasing precipitation will have an impact on future streamflow.
- With the current land cover ailments, it is anticipated that the average everyday streamflow of the Khanpur Dam will increase by 261.8 cusecs (1990–2015) to 306 cusecs for SSP2 and to 317.3 cusecs for SSP5.
- The flow increased by 313.5 cusecs under SSP2 and 327.6 cusecs under SSP5 future land cover scenarios (from 1990 to 2015).
- The results reveal that the mean monthly flows have increased generally.

This study deepened our understanding of the effects of CC and land cover change on the Khanpur Dam catchment area and showed that the impacts are significantly sufficient for project managers and planners to include them when creating long-term operating plans.

Future studies could also consider the consequences on the catchment area's groundwater and sediment alterations, even though the present research has focused on how CC and land cover change affect streamflow.

Author Contributions: All authors were involved in the intellectual elements of this paper. S.H. and M.U.M. designed the research; S.H. and M.U.M. conducted the research and wrote the manuscript; M.R., B.Đ. and C.B.P. wrote the original draft, including writing the review and editing with data arrangement, and analysis; M.S.A. participated in writing the review, editing, and formal analysis; B.Đ., R.Z.H., F.A. and I.E. participated in writing the review and editing and formal analysis. All authors have read and agreed to the published version of the manuscript.

Funding: The APC was partially funded by the scientific project "Determining the potential of watercourses for the production of electric energy from micro, mini, and pico hydropower plants" in 2023, funded by University North, Koprivnica, Croatia.

Institutional Review Board Statement: Not applicable.

Informed Consent Statement: Not applicable.

Data Availability Statement: The data is not publicly available due to further research.

Acknowledgments: The authors are thankful to the Deanship of Scientific Research at Najran University for funding this work, under the Research Groups Funding program grant code (NU/RG/SERC/12/21). The authors extend their appreciation to Abdullah Alrushaid, Chair of Earth Science Remote Sensing Research for funding. Also, the research was provided under the scientific project "Determining the potential of watercourses for the production of electric energy from micro, mini, and pico hydropower plants" in 2023 year, funded by University North, Koprivnica, Croatia.

Conflicts of Interest: The authors declare no conflict of interest.

References

1. Higashi, H.; Dairaku, K.; Matsuura, T. Impacts of Global Warming on Heavy Precipitation Frequency and Flood Risk. *Proc. Hydraul. Eng.* **2006**, *50*, 205–210. [CrossRef]
2. Watkins, K. Human Development Report 2006—Beyond Scarcity: Power, Poverty and the Global Water Crisis. 2006. Available online: https://hdr.undp.org/content/human-development-report-2006. (accessed on 10 October 2023).
3. Vörösmarty, C.J.; McIntyre, P.B.; Gessner, M.O.; Dudgeon, D.; Prusevich, A.; Green, P.; Glidden, S.; Bunn, S.E.; Sullivan, C.A.; Liermann, C.R.; et al. Global Threats to Human Water Security and River Biodiversity. *Nature* **2010**, *467*, 555–561. [CrossRef] [PubMed]
4. Kochhar, M.K.; Pattillo, M.C.; Sun, M.Y.; Suphaphiphat, M.N.; Swiston, M.A.; Tchaidze, M.R.; Clements, M.B.; Fabrizio, M.S.; Flamini, V.; Redifer, M.L.; et al. Is the Glass Half Empty or Half Full? Issues in Managing Water Challenges and Policy Instruments. *Staff Discuss. Notes* **2015**, *15*, 1. [CrossRef]
5. Gedney, N.; Cox, P.M.; Betts, R.A.; Boucher, O.; Huntingford, C.; Stott, P.A. Detection of a Direct Carbon Dioxide Effect in Continental River Runoff Records. *Nature* **2006**, *439*, 835–838. [CrossRef]
6. Lee Eun-Sung, K.S.C. Hydrological Effects of Climate Change, Groundwater Withdrawal, and Land Use in a Small Korean Watershed. *Hydrol. Process.* **2007**, *21*, 3046–3056. [CrossRef]
7. Shi, X.; Wang, W.; Shi, W. Progress on Quantitative Assessment of the Impacts of Climate Change and Human Activities on Cropland Change. *J. Geogr. Sci.* **2016**, *26*, 339–354. [CrossRef]
8. Iqbal, M.; Wen, J.; Masood, M.; Masood, M.U.; Adnan, M. Impacts of Climate and Land-Use Changes on Hydrological Processes of the Source Region of Yellow River, China. *Sustainability* **2022**, *14*, 14908. [CrossRef]
9. Du, J.; Qian, L.; Rui, H.; Zuo, T.; Zheng, D.; Xu, Y.; Xu, C.Y. Assessing the Effects of Urbanization on Annual Runoff and Flood Events Using an Integrated Hydrological Modeling System for Qinhuai River Basin, China. *J. Hydrol.* **2012**, *464*, 127–139. [CrossRef]
10. Tomer, M.D.; Schilling, K.E. A Simple Approach to Distinguish Land-Use and Climate-Change Effects on Watershed Hydrology. *J. Hydrol.* **2009**, *376*, 24–33. [CrossRef]
11. Zohaib, M.; Kim, H.; Choi, M. Evaluating the Patterns of Spatiotemporal Trends of Root Zone Soil Moisture in Major Climate Regions in East Asia. *J. Geophys. Res. Atmos.* **2017**, *122*, 7705–7722. [CrossRef]
12. Liang, W.; Bai, D.; Wang, F.; Fu, B.; Yan, J.; Wang, S.; Yang, Y.; Long, D.; Feng, M. Quantifying the Impacts of Climate Change and Ecological Restoration on Streamflow Changes Based on a Budyko Hydrological Model in China's Loess Plateau. *Water Resour. Res.* **2015**, *51*, 6500–6519. [CrossRef]
13. Trail, M.; Tsimpidi, A.P.; Liu, P.; Tsigaridis, K.; Hu, Y.; Nenes, A.; Stone, B.; Russell, A.G. Potential Impact of Land Use Change on Future Regional Climate in the Southeastern US: Reforestation and Crop Land Conversion. *J. Geophys. Res. Atmos.* **2013**, *118*, 11577–11588. [CrossRef]
14. Fohrer, N.; Haverkamp, S.; Frede, H.G. Assessment of the Effects of Land Use Patterns on Hydrologic Landscape Functions: Development of Sustainable Land Use Concepts for Low Mountain Range Areas. *Hydrol. Process.* **2005**, *19*, 659–672. [CrossRef]
15. Nasseri, M.; Zahraie, B.; Ajami, N.; Solomatine, D.P. Monthly Water Balance Modeling: Probabilistic, Possibilistic and Hybrid Methods for Model Combination and Ensemble Simulation. *J. Hydrol.* **2014**, *511*, 675–691. [CrossRef]

16. Li, Z.; Fang, H. Modeling the Impact of Climate Change on Watershed Discharge and Sediment Yield in the Black Soil Region, Northeastern China. *Geomorphology* **2017**, *293*, 255–271. [CrossRef]
17. Fernandez, R.M.; Vogel, R.M.; Sankarasubramanian, A. Regional Calibration of a Watershed Model. *Hydrol. Sci. J.* **2000**, *45*, 689–707. [CrossRef]
18. Shahid, M.; Cong, Z.; Zhang, D. Understanding the Impacts of Climate Change and Human Activities on Streamflow: A Case Study of the Soan River Basin, Pakistan. *Theor. Appl. Climatol.* **2017**, *134*, 205–219. [CrossRef]
19. Vonk, E.; Xu, Y.; Booij, M.J.; Zhang, X.M.; Augustijn, D.C. Adapting Multireservoir Operation to Shifting Patterns of Water Supply and Demand: A Case Study for the Xinanjiang-Fuchunjiang Reservoir Cascade. *Water Resour. Manag.* **2014**, *28*, 625–643. [CrossRef]
20. Masood, M.U.; Khan, N.M.; Haider, S.; Anjum, M.N.; Chen, X.; Gulakhmadov, A.; Iqbal, M.; Ali, Z.; Liu, T. Appraisal of Land Cover and Climate Change Impacts on Water Resources: A Case Study of Mohmand Dam Catchment, Pakistan. *Water* **2023**, *15*, 1313. [CrossRef]
21. Wei, X.; Liu, W.; Zhou, P. Quantifying the Relative Contributions of Forest Change and Climatic Variability to Hydrology in Large Watersheds: A Critical Review of Research Methods. *Water* **2013**, *5*, 728–746. [CrossRef]
22. Tahir, A.A.; Chevallier, P.; Arnaud, Y.; Ahmad, B. Snow Cover Dynamics and Hydrological Regime of the Hunza River Basin, Karakoram Range, Northern Pakistan. *Hydrol. Earth Syst. Sci.* **2011**, *15*, 2275–2290. [CrossRef]
23. Haider, S.; Masood, M.U.; Rashid, M.; Alshehri, F.; Pande, C.B.; Katipoğlu, O.M.; Costache, R. Simulation of the Potential Impacts of Projected Climate and Land Use Change on Runoff under CMIP6 Scenarios. *Water* **2023**, *15*, 3421. [CrossRef]
24. Yang, L.; Feng, Q.; Yin, Z.; Deo, R.C.; Wen, X.; Si, J.; Li, C. Separation of the Climatic and Land Cover Impacts on the Flow Regime Changes in Two Watersheds of Northeastern Tibetan Plateau. *Adv. Meteorol.* **2017**, *2017*, 6310401. [CrossRef]
25. Sinha, R.K.; Eldho, T.I.; Subimal, G. Assessing the Impacts of Land Use/Land Cover and Climate Change on Surface Runoff of a Humid Tropical River Basin in Western Ghats, India. *Int. J. River Basin Manag.* **2020**, *21*, 1–12. [CrossRef]
26. Ahmed, N.; Wang, G.; Booij, M.J.; Xiangyang, S.; Hussain, F.; Nabi, G. Separation of the Impact of Landuse/Landcover Change and Climate Change on Runoff in the Upstream Area of the Yangtze River, China. *Water Resour. Manag.* **2022**, *36*, 181–201. [CrossRef]
27. Nickman, A.; Lyon, S.W.; Jansson, P.E.; Olofsson, B. Simulating the Impact of Roads on Hydrological Responses: Examples from Swedish Terrain. *Hydrol. Res.* **2016**, *47*, 767–781. [CrossRef]
28. Rahman, K.U.; Balkhair, K.S.; Almazroui, M.; Masood, A. Sub-Catchments Flow Losses Computation Using Muskingum–Cunge Routing Method and HEC-HMS GIS Based Techniques, Case Study of Wadi Al-Lith, Saudi Arabia. *Model. Earth Syst. Environ.* **2017**, *3*, 4. [CrossRef]
29. Wang, G.; Zhang, J.; Pagano, T.C.; Xu, Y.; Bao, Z.; Liu, Y.; Jin, J.; Liu, C.; Song, X.; Wan, S. Simulating the Hydrological Responses to Climate Change of the Xiang River Basin, China. *Theor. Appl. Climatol.* **2015**, *124*, 769–779. [CrossRef]
30. Chu, X.; Steinman, A. Event and Continuous Hydrologic Modeling with HEC-HMS. *J. Irrig. Drain. Eng.* **2009**, *135*, 119–124. [CrossRef]
31. Tassew, B.G.; Belete, M.A.; Miegel, K. Application of HEC-HMS Model for Flow Simulation in the Lake Tana Basin: The Case of Gilgel Abay Catchment, Upper Blue Nile Basin, Ethiopia. *Hydrology* **2019**, *6*, 21. [CrossRef]
32. Gunacti, M.C.; Gul, G.O.; Cetinkaya, C.P.; Gul, A.; Barbaros, F. Evaluating Impact of Land Use and Land Cover Change Under Climate Change on the Lake Marmara System. *Water Resour. Manag.* **2022**, *37*, 2643–2656. [CrossRef]
33. Azizi, S.; Ilderomi, A.R.; Noori, H. Investigating the Effects of Land Use Change on Flood Hydrograph Using HEC-HMS Hydrologic Model (Case Study: Ekbatan Dam). *Nat. Hazards* **2021**, *109*, 145–160. [CrossRef]
34. Azmat, M.; Qamar, M.U.; Huggel, C.; Hussain, E. Future Climate and Cryosphere Impacts on the Hydrology of a Scarcely Gauged Catchment on the Jhelum River Basin, Northern Pakistan. *Sci. Total Environ.* **2018**, *639*, 961–976. [CrossRef] [PubMed]
35. Candela, L.; Tamoh, K.; Olivares, G.; Gomez, M. Modelling Impacts of Climate Change on Water Resources in Ungauged and Data-Scarce Watersheds. Application to the Siurana Catchment (NE Spain). *Sci. Total Environ.* **2012**, *440*, 253–260. [CrossRef] [PubMed]
36. Verma, A.K.; Jha, M.K.; Mahana, R.K. Evaluation of HEC-HMS and WEPP for Simulating Watershed Runoff Using Remote Sensing and Geographical Information System. *Paddy Water Environ.* **2009**, *8*, 131–144. [CrossRef]
37. Zelelew, D.G.; Melesse, A.M. Applicability of a Spatially Semi-Distributed Hydrological Model for Watershed Scale Runoff Estimation in Northwest Ethiopia. *Water* **2018**, *10*, 923. [CrossRef]
38. Karlsson, I.B.; Sonnenborg, T.O.; Refsgaard, J.C.; Trolle, D.; Børgesen, C.D.; Olesen, J.E.; Jeppesen, E.; Jensen, K.H. Combined Effects of Climate Models, Hydrological Model Structures and Land Use Scenarios on Hydrological Impacts of Climate Change. *J. Hydrol.* **2016**, *535*, 301–317. [CrossRef]
39. Li, B.; Li, C.; Liu, J.; Zhang, Q.; Duan, L. Decreased Streamflow in the Yellow River Basin, China: Climate Change or Human-Induced? *Water* **2017**, *9*, 116. [CrossRef]
40. Liu, L.; Liu, Z.; Ren, X.; Fischer, T.; Xu, Y. Hydrological Impacts of Climate Change in the Yellow River Basin for the 21st Century Using Hydrological Model and Statistical Downscaling Model. *Quat. Int.* **2011**, *244*, 211–220. [CrossRef]
41. Ahmadalipour, A.; Rana, A.; Moradkhani, H.; Sharma, A. Multi-Criteria Evaluation of CMIP5 GCMs for Climate Change Impact Analysis. *Theor. Appl. Climatol.* **2015**, *128*, 71–87. [CrossRef]

42. Rozenberg, J.; Davis, S.J.; Narloch, U.; Hallegatte, S. Climate Constraints on the Carbon Intensity of Economic Growth. *Environ. Res. Lett.* **2015**, *10*, 095006. [CrossRef]
43. Anandhi, A.; Frei, A.; Pierson, D.C.; Schneiderman, E.M.; Zion, M.S.; Lounsbury, D.; Matonse, A.H. Examination of Change Factor Methodologies for Climate Change Impact Assessment. *Water Resour. Res.* **2011**, *47*, 1–10. [CrossRef]
44. Moriasi, D.N.; Arnold, J.G.; Van Liew, M.W.; Bingner, R.L.; Harmel, R.D.; Veith, T.L. Model Evaluation Guidelines for Systematic Quantification of Accuracy in Watershed Simulations. *Trans. ASABE* **2007**, *50*, 885–900. [CrossRef]
45. Kumar, K.S.; Kumari, K.P.; Bhaskar, P.U. Application of Markov Chain & Cellular Automata Based Model for Prediction of Urban Transitions. In Proceedings of the 2016 International Conference on Electrical, Electronics, and Optimization Techniques (ICEEOT), Chennai, India, 3–5 March 2016; pp. 4007–4012.
46. Babur, M.; Babel, M.S.; Shrestha, S.; Kawasaki, A.; Tripathi, N.K. Assessment of Climate Change Impact on Reservoir Inflows Using Multi Climate-Models under RCPs—The Case of Mangla Dam in Pakistan. *Water* **2016**, *8*, 389. [CrossRef]
47. *US Army Corps of Engineers Hydrologic Modeling System HEC-HMS, Hydrologic Modeling System HEC-HMS*; User's Manual; Version 4.3; Hydrologic Engineering Centre: Davis, CA, USA, 2018; p. 640.
48. Michael Bartles, P.E. Variable Clark Unit Hydrograph Parameter Regression Equations for California. In Proceedings of the SEDHYD 2023 Conference, St. Louis, MO, USA, 8–12 May 2023.
49. Normand, A.E.; Carter, N.T. US Army Corps of Engineers: Annual Appropriations Process and Issues for Congress. CRS Report. R46320. 2020. Available online: https://sgp.fas.org/crs/natsec/R46320.pdf (accessed on 10 October 2023).
50. Kull, D.W.; Feldman, A.D. Evolution of Clark's Unit Graph Method to Spatially Distributed Runoff. *J. Hydrol. Eng.* **1998**, *3*, 9–19. [CrossRef]
51. Sparrow, K.H.; Gutenson, J.L.; Wahl, M.D.; Cotterman, K.A.; US Army Engineer Research and Development Center. *Evaluation of Climatic and Hydroclimatic Resources to Support the US Army Corps of Engineers Regulatory Program*; US Army Engineer Research and Development Center, Coastal and Hydraulics: Vicksburg, MS, USA, 2022.
52. Nasim, W.; Amin, A.; Fahad, S.; Awais, M.; Khan, N.; Mubeen, M.; Wahid, A.; Rehman, M.H.; Ihsan, M.Z.; Ahmad, S.; et al. Future Risk Assessment by Estimating Historical Heat Wave Trends with Projected Heat Accumulation Using SimCLIM Climate Model in Pakistan. *Atmos. Res.* **2018**, *205*, 118–133. [CrossRef]
53. Anjum, M.N.; Ding, Y.; Shangguan, D.; Ijaz, M.W.; Zhang, S. Evaluation of High-Resolution Satellite-Based Real-Time and Post-Real-Time Precipitation Estimates during 2010 Extreme Flood Event in Swat River Basin, Hindukush Region. *Adv. Meteorol.* **2016**, *2016*, 2604980. [CrossRef]
54. Chen, L.; Frauenfeld, O.W. Surface Air Temperature Changes over the Twentieth and Twenty-First Centuries in China Simulated by 20 CMIP5 Models. *J. Clim.* **2014**, *27*, 3920–3937. [CrossRef]
55. Kent, C.; Chadwick, R.; Rowell, D. Understanding Uncertainties in Future Projections of Seasonal Tropical Precipitation. *J. Clim.* **2015**, *28*, 150317081728001. [CrossRef]
56. Yang, T.; Hao, X.; Shao, Q.; Xu, C.-Y.; Zhao, C.; Chen, X.; Wang, W. Multi-Model Ensemble Projections in Temperature and Precipitation Extremes of the Tibetan Plateau in the 21st Century. *Glob. Planet. Change* **2012**, *80–81*, 1–13. [CrossRef]
57. Anjum, M.N.; Ding, Y.; Shangguan, D.; Ahmad, I.; Ijaz, M.W.; Farid, H.U.; Yagoub, Y.E.; Zaman, M.; Adnan, M. Performance Evaluation of Latest Integrated Multi-Satellite Retrievals for Global Precipitation Measurement (IMERG) over the Northern Highlands of Pakistan. *Atmos. Res.* **2018**, *205*, 134–146. [CrossRef]
58. Dimri, A.P.; Kumar, D.; Choudhary, A.; Maharana, P. Future Changes over the Himalayas: Maximum and Minimum Temperature. *Glob. Planet. Change* **2018**, *162*, 212–234. [CrossRef]
59. Zhang, Y.; Su, F.; Hao, Z.; Xu, C.; Yu, Z.; Wang, L.; Tong, K. Impact of Projected Climate Change on the Hydrology in the Headwaters of the Yellow River Basin. *Hydrol. Process.* **2015**, *29*, 4379–4397. [CrossRef]
60. Xin, J.; Gong, C.; Wang, S.; Wang, Y. Aerosol Direct Radiative Forcing in Desert and Semi-Desert Regions of Northwestern China. *Atmos. Res.* **2016**, *171*, 56–65. [CrossRef]
61. Gan, R.; Zuo, Q. Assessing the Digital Filter Method for Base Flow Estimation in Glacier Melt Dominated Basins. *Hydrol. Process.* **2015**, *30*, 1367–1375. [CrossRef]
62. Ozturk, T.; Turp, M.T.; Türkeş, M.; Kurnaz, M.L. Projected Changes in Temperature and Precipitation Climatology of Central Asia CORDEX Region 8 by Using RegCM4.3.5. *Atmos. Res.* **2017**, *183*, 296–307. [CrossRef]
63. Garee, K.; Chen, X.; Bao, A.; Wang, Y.; Meng, F. Hydrological Modeling of the Upper Indus Basin: A Case Study from a High-Altitude Glacierized Catchment Hunza. *Water* **2017**, *9*, 17. [CrossRef]
64. Pande, C.B.; Moharir, K.N.; Varade, A.M.; Abdo, H.G.; Mulla, S.; Yaseen, Z.M. Intertwined impacts of urbanization and land cover change on urban climate and agriculture in Aurangabad city (MS), India using google earth engine platform. *J. Clean. Prod.* **2023**, *422*, 138541. [CrossRef]
65. Anjum, M.N.; Ding, Y.; Shangguan, D.; Liu, J.; Ahmad, I.; Ijaz, M.W.; Khan, M.I. Quantification of Spatial Temporal Variability of Snow Cover and Hydro-Climatic Variables Based on Multi-Source Remote Sensing Data in the Swat Watershed, Hindukush Mountains, Pakistan. *Meteorol. Atmos. Phys.* **2018**, *131*, 467–486. [CrossRef]
66. Dahri, Z.H.; Ludwig, F.; Moors, E.; Ahmad, B.; Khan, A.; Kabat, P. An Appraisal of Precipitation Distribution in the High-Altitude Catchments of the Indus Basin. *Sci. Total Environ.* **2016**, *548*, 289–306. [CrossRef]
67. Bollasina, M.A.; Ming, Y.; Ramaswamy, V. Anthropogenic Aerosols and the Weakening of the South Asian Summer Monsoon. *Science* **2011**, *334*, 502–505. [CrossRef] [PubMed]

68. Kaskaoutis, D.G.; Houssos, E.E.; Solmon, F.; Legrand, M.; Rashki, A.; Dumka, U.C.; Francois, P.; Gautam, R.; Singh, R.P. Impact of Atmospheric Circulation Types on Southwest Asian Dust and Indian Summer Monsoon Rainfall. *Atmos. Res.* **2018**, *201*, 189–205. [CrossRef]
69. Lutz, A.F.; Immerzeel, W.W.; Shrestha, A.B.; Bierkens, M.F. Consistent Increase in High Asia's Runoff Due to Increasing Glacier Melt and Precipitation. *Nat. Clim. Change* **2014**, *4*, 587–592. [CrossRef]
70. Li, Y.; Mi, W.; Ji, L.; He, Q.; Yang, P.; Xie, S.; Bi, Y. Urbanization and Agriculture Intensification Jointly Enlarge the Spatial Inequality of River Water Quality. *Sci. Total Environ.* **2023**, *878*, 162559. [CrossRef] [PubMed]
71. Yang, D.; Qiu, H.; Ye, B.; Liu, Y.; Zhang, J.; Zhu, Y. Distribution and Recurrence of Warming-Induced Retrogressive Thaw Slumps on the Central Qinghai-Tibet Plateau. *J. Geophys. Res. Earth Surf.* **2023**, *128*, e2022JF007047. [CrossRef]
72. Sang, L.; Zhu, G.; Xu, Y.; Sun, Z.; Zhang, Z.; Tong, H. Effects of Agricultural Large-And Medium-Sized Reservoirs on Hydrologic Processes in the Arid Shiyang River Basin, Northwest China. *Water Resour. Res.* **2023**, *59*, e2022WR033519. [CrossRef]
73. Li, J.; Wang, Z.; Wu, X.; Xu, C.-Y.; Guo, S.; Chen, X. Toward Monitoring Short-Term Droughts Using a Novel Daily Scale, Standardized Antecedent Precipitation Evapotranspiration Index. *J. Hydrometeorol.* **2020**, *21*, 891–908. [CrossRef]
74. Li, W.; Wang, C.; Liu, H.; Wang, W.; Sun, R.; Li, M.; Shi, Y.; Zhu, D.; Du, W.; Ma, L. Fine Root Biomass and Morphology in a Temperate Forest Are Influenced More by Canopy Water Addition than by Canopy Nitrogen Addition. *Front. Ecol. Evol.* **2023**, *11*, 1132248. [CrossRef]
75. Wu, B.; Quan, Q.; Yang, S.; Dong, Y. A Social-Ecological Coupling Model for Evaluating the Human-Water Relationship in Basins within the Budyko Framework. *J. Hydrol.* **2023**, *619*, 129361. [CrossRef]
76. Yang, Y.; Liu, L.; Zhang, P.; Wu, F.; Wang, Y.; Xu, C.; Zhang, L.; An, S.; Kuzyakov, Y. Large-Scale Ecosystem Carbon Stocks and Their Driving Factors across Loess Plateau. *Carbon Neutrality* **2023**, *2*, 5. [CrossRef]
77. Fang, Y.-K.; Wang, H.-C.; Fang, P.-H.; Liang, B.; Zheng, K.; Sun, Q.; Li, X.-Q.; Zeng, R.; Wang, A.-J. Life Cycle Assessment of Integrated Bioelectrochemical-Constructed Wetland System: Environmental Sustainability and Economic Feasibility Evaluation. *Resour. Conserv. Recycl.* **2023**, *189*, 106740. [CrossRef]
78. Xu, Z.; Li, X.; Li, J.; Xue, Y.; Jiang, S.; Liu, L.; Luo, Q.; Wu, K.; Zhang, N.; Feng, Y. Characteristics of Source Rocks and Genetic Origins of Natural Gas in Deep Formations, Gudian Depression, Songliao Basin, NE China. *ACS Earth Sp. Chem.* **2022**, *6*, 1750–1771. [CrossRef]
79. Gao, C.; Hao, M.; Chen, J.; Gu, C. Simulation and Design of Joint Distribution of Rainfall and Tide Level in Wuchengxiyu Region, China. *Urban Clim.* **2021**, *40*, 101005. [CrossRef]
80. Zhou, G.; Lin, G.; Liu, Z.; Zhou, X.; Li, W.; Li, X.; Deng, R. An Optical System for Suppression of Laser Echo Energy from the Water Surface on Single-Band Bathymetric LiDAR. *Opt. Lasers Eng.* **2023**, *163*, 107468. [CrossRef]
81. Zhou, G.; Wu, G.; Zhou, X.; Xu, C.; Zhao, D.; Lin, J.; Liu, Z.; Zhang, H.; Wang, Q.; Xu, J. Adaptive Model for the Water Depth Bias Correction of Bathymetric LiDAR Point Cloud Data. *Int. J. Appl. Earth Obs. Geoinf.* **2023**, *118*, 103253. [CrossRef]
82. Zhou, G.; Yang, Z. Analysis for 3-D Morphology Structural Changes for Underwater Topographical in Culebrita Island. *Int. J. Remote Sens.* **2023**, *44*, 2458–2479. [CrossRef]
83. Luo, J.; Niu, F.; Lin, Z.; Liu, M.; Yin, G.; Gao, Z. Abrupt Increase in Thermokarst Lakes on the Central Tibetan Plateau over the Last 50 Years. *Catena* **2022**, *217*, 106497. [CrossRef]
84. Gong, S.; Bai, X.; Luo, G.; Li, C.; Wu, L.; Chen, F.; Ran, C.; Xi, H.; Zhang, S. Climate Change Has Enhanced the Positive Contribution of Rock Weathering to the Major Ions in Riverine Transport. *Glob. Planet. Change* **2023**, *228*, 104203. [CrossRef]
85. Ran, C.; Bai, X.; Tan, Q.; Luo, G.; Cao, Y.; Wu, L.; Chen, F.; Li, C.; Luo, X.; Liu, M. Threat of Soil Formation Rate to Health of Karst Ecosystem. *Sci. Total Environ.* **2023**, *887*, 163911. [CrossRef]
86. Zhu, X.; Xu, Z.; Liu, Z.; Liu, M.; Yin, Z.; Yin, L.; Zheng, W. Impact of Dam Construction on Precipitation: A Regional Perspective. *Mar. Freshw. Res.* **2022**, *74*, 877–890. [CrossRef]
87. Liu, Z.; Xu, J.; Liu, M.; Yin, Z.; Liu, X.; Yin, L.; Zheng, W. Remote Sensing and Geostatistics in Urban Water-Resource Monitoring: A Review. *Mar. Freshw. Res.* **2023**, *74*, 747–765. [CrossRef]
88. Yin, L.; Wang, L.; Ge, L.; Tian, J.; Yin, Z.; Liu, M.; Zheng, W. Study on the Thermospheric Density Distribution Pattern during Geomagnetic Activity. *Appl. Sci.* **2023**, *13*, 5564. [CrossRef]
89. Yin, L.; Wang, L.; Li, T.; Lu, S.; Yin, Z.; Liu, X.; Li, X.; Zheng, W. U-Net-STN: A Novel End-to-End Lake Boundary Prediction Model. *Land* **2023**, *12*, 1602. [CrossRef]
90. Yin, Z.; Liu, Z.; Liu, X.; Zheng, W.; Yin, L. Urban Heat Islands and Their Effects on Thermal Comfort in the US: New York and New Jersey. *Ecol. Indic.* **2023**, *154*, 110765. [CrossRef]
91. Kisi, O.; Choubin, B.; Deo, R.C.; Yaseen, Z.M. Incorporating Synoptic-Scale Climate Signals for Streamflow Modelling over the Mediterranean Region Using Machine Learning Models. *Hydrol. Sci. J.* **2019**, *64*, 1240–1252. [CrossRef]
92. Malik, S.; Malik, S. Maternal Influence on Youth Radicalization–A Case Study of District Multan. *J. Contemp. Stud.* **2021**, *10*, 38–58.
93. Halder, B.; Ameen, A.M.S.; Bandyopadhyay, J.; Khedher, K.M.; Yaseen, Z.M. The Impact of Climate Change on Land Degradation along with Shoreline Migration in Ghoramara Island, India. *Phys. Chem. Earth Parts A/B/C* **2022**, *126*, 103135. [CrossRef]
94. Abd Alraheem, E.; Jaber, N.A.; Jamei, M.; Tangang, F. Assessment of Future Meteorological Drought under Representative Concentration Pathways (RCP8. 5) Scenario: Case Study of Iraq. *Knowl. Based Eng. Sci.* **2022**, *3*, 64–82.
95. Bandyopadhyay, J.; Rahaman, S.K.H.; Karan, C. Agricultural Potential Zone Mapping with Surface Water Resource Management Using Geo-Spatial Tools for Jhargram District, West Bengal, India. *Knowl. Based Eng. Sci.* **2023**, *4*, 1–18.

96. Immerzeel, W.W.; Van Beek, L.P.H.; Konz, M.; Shrestha, A.B.; Bierkens, M.F.P. Hydrological Response to Climate Change in a Glacierized Catchment in the Himalayas. *Clim. Change* **2012**, *110*, 721–736. [CrossRef]
97. Immerzeel, W.W.; Pellicciotti, F.; Bierkens, M.F. Rising River Flows throughout the Twenty-First Century in Two Himalayan Glacierized Watersheds. *Nat. Geosci.* **2013**, *6*, 742–745. [CrossRef]
98. Immerzeel, W.W.; Wanders, N.; Lutz, A.F.; Shea, J.M.; Bierkens, M.F.P. Reconciling High-Altitude Precipitation in the Upper Indus Basin with Glacier Mass Balances and Runoff. *Hydrol. Earth Syst. Sci.* **2015**, *19*, 4673–4687. [CrossRef]